energies

Article

Experimental Study and Reaction Pathway Analysis of Solvothermal Directional Conversion of Pyrolysis Crude Oil to Liquid Fuel

Qi Wei, Zhongyang Luo *, Qian Qian, Jingkang Shi and Feiting Miao

State Key Laboratory of Clean Energy Utilization, Zhejiang University, Hangzhou 310027, China
* Correspondence: zyluo@zju.edu.cn; Tel.: +86-571-87952440

Abstract: The high viscosity and oxygen content of pyrolysis crude oil hinder the advancement of pyrolysis technology. To address the issue, this study conducted hydrodeoxygenation upgrading experiments on pyrolysis crude oil using hydrothermal directional conversion. A variable analysis was performed to assess the differences in upgrading effects based on the active metal (Ru, Pt) and the supports (activated carbon, Nb_2O_5, MgO) of the supported catalyst, and further investigations were conducted on the catalyst with bimetallic doping modification. Optimal reaction conditions were determined by adjusting the reaction temperature. Additionally, directional conversion studies of model compounds were carried out to elucidate the reaction pathway. The results indicated that the Pt/MgO catalyst achieved the highest yield of stable and combustible compounds (hydrocarbons, alcohols, ethers, esters, and ketones), with a yield of 17.8 wt%. Upon modification with Ni doping, the yield increased by 49.5%. The upgrading effect improved with an increase in reaction temperature, and the yield of target compounds was 26.7 wt% at 290 °C, with an energy conversion rate of 72.6% and a selectivity of 75.8%. Moreover, the physicochemical properties of the upgraded oil were similar to those of ethanol. All three model compounds underwent 100% conversion. This study provides both experimental support and a theoretical foundation for the further development of biomass conversion technology.

Keywords: pyrolysis crude oil; solvothermal directional conversion; catalyst screening; reaction pathway; liquid fuel

Academic Editor: Wenzhi Li

Received: 29 December 2024
Revised: 3 February 2025
Accepted: 16 February 2025
Published: 18 February 2025

Citation: Wei, Q.; Luo, Z.; Qian, Q.; Shi, J.; Miao, F. Experimental Study and Reaction Pathway Analysis of Solvothermal Directional Conversion of Pyrolysis Crude Oil to Liquid Fuel. *Energies* **2025**, *18*, 981. https://doi.org/10.3390/en18040981

1. Introduction

Recently, the rapid advancement of human society and industrialization has increased the need for energy, posing unprecedented challenges to the environment [1]. Currently, fossil fuels remain the primary energy source for many countries [2,3]. The extensive use of these fuels not only results in energy shortages and exacerbates global disputes and instability [4], but also contributes to significant pollutant emissions, causing detrimental effects to the environment [5]. To tackle this issue, the development of renewable energy sources is of paramount importance [6]. Among numerous renewable resources, biomass displays a variety of advantages such as renewability, conversion into liquid fuel, and negative carbon emissions [7]. It has become an important force in the transformation of global energy structures. Biomass refers to various organisms formed through photosynthesis and has a rich composition, including crops, wood, agricultural and forestry waste, as well as animal manure [8,9]. Biomass is the sole renewable resource in nature that can be directly transformed into carbon-based liquid fuel [10,11]. Transforming biomass into clean

and high-quality liquid fuel is an important process that can balance the contradictory of sustainable development needs and the constantly increasing energy demand [12].

There are various ways to utilize biomass. Fast pyrolysis is a process in which biomass is rapidly heated to high temperatures (usually between 450 °C and 600 °C) in an oxygen-free or low-oxygen environment [13,14]. This technology can achieve full component utilization of biomass and has strong adaptability to raw materials. Fast pyrolysis has become a highly promising technological route [15,16]. However, the pyrolysis crude oil obtained through fast pyrolysis has complex components, including acids, aldehydes, ketones, phenols, and their oligomers [17]. These components cause the oil to have a high oxygen content, low pH, reduced heat of combustion, as well as inadequate stability, which seriously affects the practical application of pyrolysis crude oil [18,19]. Therefore, conducting targeted conversion research on pyrolysis crude oil to further improve its quality is crucial to promote the high-value utilization of biomass.

Among various quality improvement methods, catalytic hydrodeoxygenation can effectively reduce the oxygen concentration of pyrolysis crude oil and obtain premium bio-oil, which has received widespread attention [20,21]. During the hydrodeoxygenation reaction, catalysts have a significant impact on the effectiveness of upgrading [22]. Research has found that metal catalysts, which can promote the dissociation of hydrogen, have a better ability to activate hydrogen compared to non-metal catalysts, thereby facilitating the occurrence of hydrogenation, hydrocracking, dehydrogenation, and decarbonylation reactions [23,24]. Common catalysts include precious metal catalysts (such as Rh, Ru, Pt, and Pd), transition metal catalysts (such as Ni, Mo, W, and Co), and their corresponding bimetallic catalysts [25–27]. Current research has demonstrated that transition metal Ni, as well as precious metals Pt and Pd, possess exceptionally outstanding hydrogenation capabilities. Saidi et al. [28] prepared a new, stable type of nickel molybdenum nanoparticle catalyst and conducted an aqueous phase upgrading reaction of the pyrolysis crude oil model compound anisole. The study found that the catalyst had excellent activity in converting phenolic compounds into deoxygenated liquid fuel. Shi et al. [29] employed a one-pot approach to study the hydrodeoxygenation reaction of pyrolysis crude oil and demonstrated that under mild conditions (300 °C, 5 MPa H_2), high-quality hydrocarbons up to 81.6 C% could be obtained using Ni/ZrO_2 as the catalyst and supercritical cyclohexane as the solvent. Natsume et al. [30] conducted a study on the ex situ catalytic fast pyrolysis of cedar chips, comparing the catalytic activity of seven catalysts: Ni_2P/SiO_2, Ni_2P/ZSM-5, Ni/SiO_2, SiO_2, silica–alumina, ZSM-5 zeolite, and FCC. Among these, Ni_2P/SiO_2 exhibited the best performance, reducing the oxygen content of the upgraded bio-oil to approximately half of its original level. Wang et al. [31] studied the purification of two crude bio-oils obtained from fast pyrolysis and catalytic pyrolysis. The outcomes indicated that Pt/MZ-5 had good reaction efficiency, with a significant reduction in the oxygen content of the bio-oil. Yang et al. [32] used oil–water amphiphilic Pd/carbon–silica–alumina catalysts to explore the hydrogenation reaction of phenol. At 200 °C, the phenol conversion rate peaked at 98.0%, and its selectivity for cyclohexane was 87.7%. Zhang et al. [33] prepared two catalysts, Ni/SiO_2 and Ni/γ-Al_2O_3, and found that the model compound phenol could achieve a conversion rate of 99% at 300 °C. Additionally, the selectivity of cyclohexane could reach 90%.

In addition, the selection of catalyst supports is crucial. Existing studies have shown that the use of alkaline catalyst supports or the addition of solid bases during the reaction process can facilitate the conversion of biomass platform molecules [6]. Alkali and alkaline earth metals promote the formation of furans and ketones through ring cleavage and dehydration reactions [34]. Wang et al. [35] found in their research on ex situ catalytic fast pyrolysis of bao residue and waste lubricating oil that MgO effectively promotes deacidi-

fication through ketonization and aldol condensation reactions, resulting in a maximum aromatic yield of 39.398%. Lin et al. [36] found that MgO can promote the cleavage of long polymer chains, thereby increasing olefin yields. Long et al. [37] demonstrated that MgO can adsorb phenolic hydroxyl groups and promote the demethoxylation of guaiacol. Concurrently, several studies have indicated that acidic sites can form strong interactions with oxygen atoms, facilitating the adsorption of reactants and thereby promoting the production of fully deoxygenated products [38]. Li et al. [39] demonstrated that Nb_2O_5 prepared in their laboratory exhibited significantly higher activity in the one-pot hydrodeoxygenation of lignin monomers compared to commercially purchased Nb_2O_5. This enhanced activity was primarily attributed to the presence of both strong Lewis and Brønsted acid sites in the lab-prepared Nb_2O_5. Similarly, Leal et al. [40] achieved 88% selectivity for cyclohexane in the hydrodeoxygenation of diphenyl ether by adjusting the acidity of the Ni/Nb_2O_5 catalyst.

It is evident that scholars have conducted extensive studies on the hydrodeoxygenation of pyrolysis crude oil model compounds. However, due to the complex composition of actual pyrolysis crude oil, related research remains limited, and the reaction pathways are not yet fully understood. Moreover, the catalyst remains a bottleneck in the hydrodeoxygenation process, and the preparation and selection of high-performance catalysts continue to be a challenge. Additionally, the current reaction conditions for the purification of pyrolysis crude oil are still demanding, with reaction temperatures typically ranging from 300 °C to 450 °C and pressures from 7 to 20 MPa [41].

In summary, the complex composition of pyrolysis crude oil results in a relatively low conversion rate, and most related studies are confined to the use of model compounds rather than actual feedstock. To address this issue, this paper conducts solvothermal experimental research on the directional conversion of actual pyrolysis crude oil. Specifically, "directional conversion" refers to the targeted and controlled transformation of pyrolysis oil into specific desired products through the solvothermal process, namely stable and combustible compounds (hydrocarbons, alcohols, ethers, esters, and ketones). By optimizing reaction conditions and selecting appropriate catalysts, this study aims to guide the conversion pathways to produce high-value liquid fuels while minimizing the formation of undesired byproducts. At the same time, to further clarify the reaction process, the reaction pathways of model compounds were explored, thereby providing theoretical guidance and reference directions for subsequent improvements. This research is significant for both the theoretical advancement and commercial application of biomass pyrolysis technology.

2. Materials and Methods

2.1. Material Sources and Characterization

The pyrolysis crude oil employed in this research is the liquid phase product derived from cotton stalks after pyrolysis, which comes from the fluidized-bed continuous fast pyrolysis plant of the University of Science and Technology of China. The pyrolysis was conducted at 500 °C. N_2 was used as the fluidizing gas at a flow rate of 0.5 L/s, and the feeding rate of cotton stalk particles was 2.1 g/min [42].

The collected pyrolysis crude oil was directly characterized using gel permeation chromatography (GPC) (Agilent PL-GPC50 & Agilent 1260, Santa Clara, CA, USA), gas chromatography (Agilent 8860, Santa Clara, CA, USA) coupled with mass spectrometry (Agilent 5977B, Santa Clara, CA, USA) (GC–MS), Fourier transform infrared spectroscopy (FT-IR) (Thermo Scientific Nicolet iS20, Waltham, MA, USA), and elemental analysis (Thermo Scientific Flash 2000, Waltham, MA, USA). The GPC detection technique allows for an in-depth understanding of the molecular weight distribution in the pyrolysis crude oil. The GC–MS detection technique enables the accurate determination of the chemical formulas

and molecular structures of compounds in the pyrolysis crude oil in a relatively short period, facilitating qualitative and quantitative analysis. FT-IR technology can identify the functional groups present in the pyrolysis crude oil based on characteristic frequencies in the infrared absorption spectrum, thereby determining the category of unknown compounds. Through elemental analysis, it is possible to determine the types and amounts of various elements in the pyrolysis crude oil, thereby assessing the quality and usability of the oil.

2.2. Catalyst Preparation

Ru/C was a directly purchased commercially available catalyst with a loading capacity of 5 wt%. Before use, the catalyst was dehydrated overnight at 90 °C, then underwent reduction at 400 °C for 4 h with a hydrogen flow rate of 100 mL/min H_2, and finally passivated for 1 h at ambient temperature in a 0.5% O_2–N_2 atmosphere.

The Nb_2O_5 support was synthesized using a hydrothermal technique, and the loading of Ru was carried out using the equal volume impregnation method with a loading amount of 2 wt%. Firstly, we dissolved 1 g of cetyltrimethylammonium bromide in 15 mL of deionized water and prepared the template solution. Then we dissolved 20 mmol of $NbCl_5$ precursor salt solution in 20 mL of ethanol, vigorously agitated for 10 min until the mixture turned clear, and then added it dropwise to the template solution. After mixing, the solution was agitated for 0.5 h. Subsequently, we added 20 mL of hydrochloric acid aqueous solution to the mixed solution and agitated further for 1.5 h. After stirring, we aged the solution in a 150 °C oven for 24 h. The aged solid was isolated using centrifugation and rinsed with water till reaching a neutral pH. Then, the obtained solid was placed in a 60 °C oven to dry overnight. After drying, the solid was calcined at 450 °C for 6 h, with a heating rate of 1 °C/min. Upon reaching room temperature, the Nb_2O_5 support was obtained. We measured the water absorption of Nb_2O_5, prepared the corresponding $RuCl_2$ solution, added $RuCl_2$ solution dropwise to Nb_2O_5, and stirred continuously with a spoon to ensure uniform loading. Next, we repeated vacuum pumping and ultrasonic vibration three times to remove air from the support pores and distributed metal active sites inside the support pores. Then the material was reduced at 400 °C for 4 h with a flow rate of 100 mL/min H_2, and finally passivated at ambient temperature in a 0.5% O_2–N_2 atmosphere for 1 h.

The Ru/MgO, Pt/MgO, and Pt–Ni/MgO catalysts were synthesized utilizing an equal volume impregnation approach, with loadings of Ru and Pt at 2 wt% each, and Ni at 10 wt%. After determining the water absorption rate of MgO, a certain amount of $RuCl_3 \cdot 3H_2O$, $H_2PtCl_6 \cdot 6H_2O$, or $Ni(NO_3)_2 \cdot 6H_2O$ aqueous solution was prepared according to the catalyst configuration, and impregnated into MgO using the aforementioned equal volume impregnation method. After ultrasonication for 1 h, it was left to stand overnight at a temperature of 110 °C. It was heated to 400 °C for 2 h, followed by reduction at 500 °C for 2 h under a flow rate of 100 mL/min H_2, with a heating rate of 1 °C/min. Finally, it was passivated for 1 h at ambient temperature in a 0.5% O_2–N_2 atmosphere.

2.3. Catalyst Characterization

The characterization of catalysts serves a crucial function in the study of the solvothermal conversion of pyrolysis crude oil. In this study, the following methods were employed to characterize the prepared Pt–Ni/MgO catalyst.

Nitrogen adsorption–desorption isotherms can provide information on the specific surface area. In this study, a gas adsorption analyzer (ASAP 2460, Micromeritics, Norcross, GA, USA) was utilized for nitrogen adsorption–desorption analysis. To guarantee the precision of the test, the material was degassed at 200 °C for 8 h before the experiment to remove adsorbed impurities and moisture. During data analysis, the surface area was

estimated using the Brunauer–Emmett–Teller (BET) equation. The pore size distribution was estimated through the Barrett–Joyner–Halenda (BJH) method.

The apparent morphology and structure of the catalyst were analyzed with a scanning electron microscope (ZEISS Sigma 300, Oberkochen, Baden-Württemberg, Germany), which also allowed for the observation of the distribution of substances. During testing, a small amount of the sample was adhered to conductive adhesive, and then gold-sprayed at 10 mA using a Quorum SC7620 sputter coater (Rye, East Sussex, UK). Subsequently, images were captured using the scanning electron microscope. The acceleration voltage was set at 3 kV for morphological imaging and 15 kV for energy spectrum mapping, with the SE2 secondary electron detector being used.

The crystal structure of the catalyst was analyzed using an X-ray diffractometer (Bruker D8 Advance, Karlsruhe, Baden-Württemberg, Germany). A monochromatic Cu–Kα radiation source was used, with a step size of 0.01°, an integration time of 0.3 s/step, and a scanning diffraction angle 2θ of 10–80°. The experiment was carried out at 40 mA and 40 kV.

To further study the state of the metals, the valence states of the catalyst were examined using X-ray photoelectron spectroscopy (Thermo Scientific K-Alpha, Waltham, MA, USA). The catalyst was pressed into a pellet and attached to the sample plate, which was then inserted in the sample chamber. When the pressure dropped below 5.0×10^{-7} mbar, the sample was sent for analysis. The experiment used a monochromatic radiation source (Al–Kα), with a spot size of 400 μm, a working voltage of 12 kV, and a filament current of 6 mA; the narrow spectrum scan pass energy was 50 eV, with a step size of 0.1 eV. The C1s peak at 284.80 eV was used as the energy standard for binding energy to correct for shifts caused by the charge effect. The peak shape was analyzed using the Shirley type background correction method, and curve fitting was performed using the Gaussian–Lorentzian function.

2.4. Solvothermal Experimental Methods and Products Analysis

All experiments in this study were conducted in a 50 mL high-pressure solvothermal reactor produced by Labe Instrument. During the catalyst screening experiment, 0.2 g of catalyst and 2 mL of pyrolysis crude oil were introduced into the reactor, followed by the addition of 20 mL of ethanol as a solvent. After sealing the reactor, hydrogen was used to purge three times, and then 0.5 MPa of hydrogen was added. The reaction was conducted at 290 °C for 5 h, and the stirring speed was 800 rpm. Using centrifugation, the solid and liquid phase were separated following the reaction. The solid was rinsed with ethanol, dried overnight, and then weighed. The liquid phase was analyzed qualitatively by GC–MS and quantitatively using the external standard method. During the reaction system optimization study, the temperature was set at 250 °C, 270 °C, and 290 °C in turn, with all other operating conditions being the same as described above.

The formulas for $Yield_t$, $Energy\ Conversion\ Rate_t$, and $Selectivity_t$ of target compounds are as follows:

$$Yield_t = \frac{m_t}{m_{pyrolysis\ crude\ oil}} \tag{1}$$

$$Energy\ Conversion\ Rate_t = \frac{\sum_i (m_i \times q_i)}{m_{pyrolysis\ crude\ oil} \times q_{pyrolysis\ crude\ oil}} \tag{2}$$

$$Selectivity_t = \frac{Peak\ Area_t}{Peak\ Area_{total}} \tag{3}$$

where m_t represents the total mass of the target compounds after upgrading. Among various components, acids can increase the corrosiveness of the oil, affecting its promotion and application. Aldehydes are unstable and prone to oligomerization and condensation

reactions, which impact the stability of the fuel. Phenolic substances are not stable enough during storage and transportation, as they are likely to undergo oxidation or polymerization reactions and possess higher toxicity. These three types of substances are not suitable for use as liquid fuel. The ketones, esters, alcohol ethers, and hydrocarbons present in the oil are relatively stable and flammable, thus they are considered the target compounds in this study; $m_{pyrolysis\ crude\ oil}$ denotes the total mass of the pyrolysis crude oil before the reaction; m_i represents the mass of each target compounds; q_i denotes the calorific value of each target compounds; $q_{pyrolysis}$ crude oil refers to the calorific value of the pyrolysis crude oil; $Peak\ Area_t$ refers to the total peak area of the target compounds detectable by GC, while $Peak\ Area_{total}$ indicates the cumulative peak area of all liquid phase substances detected by GC.

The non-condensable gases obtained after the reaction were qualitatively and quantitatively analyzed. The gas phase components were analyzed using an Agilent 8860 gas chromatograph (GC) equipped with a flame ionization detector (FID) and a thermal conductivity detector (TCD). The GC utilized an HP-PLOT-Al_2O_3 column to separate the different components in the gas sample. The column oven temperature program was set to hold at 70 °C for 5.5 min, then ramp up at 20 °C/min to 130 °C, and hold for 1.5 min. Quantitative analysis of the gas components was performed using the external standard method.

The upgraded oil was vacuum evaporated at 50 °C to remove solvents, dehydrated using 3A molecular sieves, and then subjected to physical and chemical property testing. Density measurements were conducted using a hydrometer. The kinematic viscosity was determined with the SYD-265C kinematic viscometer for petroleum products, manufactured by Shanghai Changji Geological Instrument Co., Ltd., Shanghai, China. The calorific value was ascertained using the SDC712 type oxygen bomb calorimeter (Sande, Suzhou, China). The pH value was determined using a PHS-3C precision pH meter from Shanghai Laichi Instrument Factory, Shanghai, China.

3. Results and Discussion

3.1. Characterization Results of Pyrolysis Crude Oil

The main substances in the GC–MS analysis results of pyrolysis crude oil are shown in Table 1, and all substances along with their proportions are shown in the Appendix A Table A1. It can be observed that phenols account for the highest proportion, which is 68.06%, mainly originating from the pyrolysis of lignin and the transformation of its related derivatives. Phenols are difficult to burn and have low energy output, severely affecting the performance of the oil. Additionally, alcohols/ethers, ketones, and acids also account for a certain proportion, with alcohols/ethers and ketones being relatively stable and combustible, accounting for 18.76% and 6.11%, respectively. Alcohols/ethers and ketones can be considered as target compounds for oil upgrading. Acids, which mainly come from the pyrolysis of hemicellulose with acetic acid being the main component, account for 6.04%. The presence of acids increases the corrosiveness of the oil, affecting the promotion and application of the fuel. Therefore, the transformation and quality improvement of phenols and acids should be given priority consideration.

The elemental analysis results of pyrolysis crude oil are as follows: C (20.20%), H (8.87%), O (70.93%), N (0%), and S (0%). It can be observed that the pyrolysis crude oil has a high oxygen content, which leads to a reduction in the energy density of the oil. At the same time, fuels with high oxygen content produce more water vapor during combustion, which may affect the composition of the exhaust gases and increase the corrosiveness during the combustion process. Therefore, the hydrodeoxygenation and quality improvement of the pyrolysis crude oil are necessary for the practical application of biomass pyrolysis technology.

Table 1. Main substances in the GC–MS analysis results of pyrolysis crude oil.

Substance Type	Relative Peak Area (%)
Alcohols/Ethers	
Ethanol	16.59
Melezitose	2.17
Ketones	
1,2-Cyclopentanedione, 3-methyl-	2.95
Phenols	
Catechol	6.17
Phenol, 3-methyl-	6.00
Phenol	4.91
1,2-Benzenediol, 4-methyl-	4.65
Phenol, 2-methoxy-	4.46
Phenol, 2,6-dimethoxy-	3.90
Creosol	3.53
trans-Isoeugenol	3.25
Phenol, 2-methyl-	3.02
4-Ethylcatechol	2.36
Phenol, 2,6-dimethyl-	2.28
3,5-Dimethoxy-4-hydroxytoluene	2.15
Phenol, 4-ethyl-	2.05
Phenol, 4-ethyl-2-methoxy-	2.02
Acids	
Acetic acid	6.04

The GPC spectrum of the pyrolysis crude oil is shown in Figure A1. Analysis shows there are two different peaks in the oil sample, one in the high molecular weight (HMW) range and one in the low molecular weight (LMW) range. After peak separation and analysis of the chromatogram, the molecular information obtained is shown in Table 2.

Table 2. GPC molecular information of pyrolysis crude oil.

Peak Pattern	Average Molecular Weight M_w	Number Average Molecular Weight M_n	PDI	Peak Area (mV·s)
HMW	1018	945	1.08	54.32
LMW	325	286	1.14	422.08

The PDI values (M_w/M_n) of the two peaks are close to 1, indicating a narrow dispersion, which proves that the distribution range of molecular weight within the peak is narrow. The HMW peak in the sample is believed to consist primarily of polymer molecules, polycyclic aromatic hydrocarbons, tar, and coke, while the LMW peak is mainly composed of simple monomers, complex monomers, and dimer molecules [43]. At the same time, it can be found that the area ratio of the LMW peak to the HMW peak is 7.77, which suggests that most of the substances in the actual pyrolysis crude oil are within the LMW range. This may be due to the short reaction time of the pyrolysis process and the production of a large amount of water, which to a certain extent inhibits the further condensation of simple monomers, allowing substances with lower molecular weights to be retained. In summary, the actual pyrolysis crude oil can retain the monocyclic structure well and has the potential for further utilization.

3.2. Catalyst Screening

Catalysts play a crucial role in the effectiveness of the hydrodeoxygenation reaction. Therefore, this study investigated the differences in product quality under different catalyst

supports and loading types. To compare the effects of catalyst supports on the upgrading of pyrolysis crude oil, this study carried out related experimental research using neutral activated carbon, acidic oxide Nb_2O_5, and alkaline oxide MgO loaded with metal Ru, which have been confirmed to have superior effects. The main reaction products are shown in Table 3, with all substances and their proportions listed in Appendix A Table A2, and the distribution of the products is shown in Figure 1.

Table 3. Main substances in the GC–MS analysis results of upgraded oil after reaction of various catalyst supports.

Substance	Relative Peak Area (%)		
	Ru/C	Ru/Nb_2O_5	Ru/MgO
Hydrocarbons			
Dodecane			1.57
Alcohols/Ethers			
1-Butanol	22.18	10.44	23.96
Ethyl ether	2.74	3.79	
Ethane, 1,1-diethoxy-	4.42	8.37	12.30
Furan, 2,5-dihydro-			5.00
Crotonyl alcohol			4.92
1-Hexanol			1.56
Esters			
Ethyl Acetate	18.90	27.37	13.56
Butanoic acid, ethyl ester	1.60	1.67	2.19
Butyl acetate			2.45
Ketones			
Butanal			1.56
Aldehyde			
Acetaldehyde	23.30	14.09	10.90
Propanal, 2-methyl-		4.94	
Phenols			
Phenol	2.25	2.78	3.15
Phenol, 2-methoxy-	2.10	0.61	0.95
Phenol, 2-methyl-	1.58	1.70	1.79
Phenol, 3-methyl-	1.79	1.45	3.86
Creosol	1.85	0.94	0.89
Phenol,4-ethyl-2-methoxy-	2.55	0.85	
Phenol,2-methoxy-4-propyl-	3.39	1.16	1.23
Phenol, 4-ethyl-	0.52	0.78	1.54
Phenol, 2-ethoxy-		1.51	
2-Ethoxy-4-methylphenol		3.60	
Benzene, 1-ethoxy-2-methoxy-4-methyl-		2.56	

It can be observed that the composition of the upgraded oils obtained from the reactions with the three catalysts showed significant improvement compared to the pyrolysis crude oil. The selectivity of target compounds in the pyrolysis crude oil was 25.9%, with phenols being the major component, accounting for as much as 68.06%. Correspondingly, when C and Nb_2O_5 are used as supports, the selectivity of the target compounds is similar, at 58.7% and 58.2%, respectively. When using MgO as a support, the proportion of target compounds reaches to the maximum amount of 73.4%. At this time, the selectivity of aldehydes and phenolic substances that cannot be used as fuel is the lowest. The proportion of alcohol/ether substances in the products of the three different catalyst supports is in the order of MgO > C > Nb_2O_5, and the proportion of ester substances is in the order of Nb_2O_5 > C > MgO. It has been speculated that the alkaline support is more conducive to the etherification of acidic components (such as carboxylic acids and phenols) in pyrolysis

crude oil to obtain ether substances, and the hydrogenation reduction of aldehydes and ketones to produce alcohol substances, so the alkaline support also has a higher deoxygenation efficiency [35,37]. The acidic support is more likely to cause carboxylic acids, aldehydes, and ketones to undergo esterification with alcohol substances to produce ester substances. Further analysis shows that this is because alkaline substances usually tend to promote proton transfer and weakening of hydrogen bonds, thereby increasing the activity of reactants and making the reaction more likely to proceed in the direction of producing alcohols and ethers. Acidic substances usually tend to promote the protonation of carbonyl oxygen atoms, thereby activating carbonyl compounds and making the reaction more likely to proceed in the direction of producing esters. Current research has shown that a catalyst with a greater alkalinity level is beneficial for decarboxylation, while a higher acidity helps break C-O, C-H, and O-H bonds, thereby reducing alcohol substances [44].

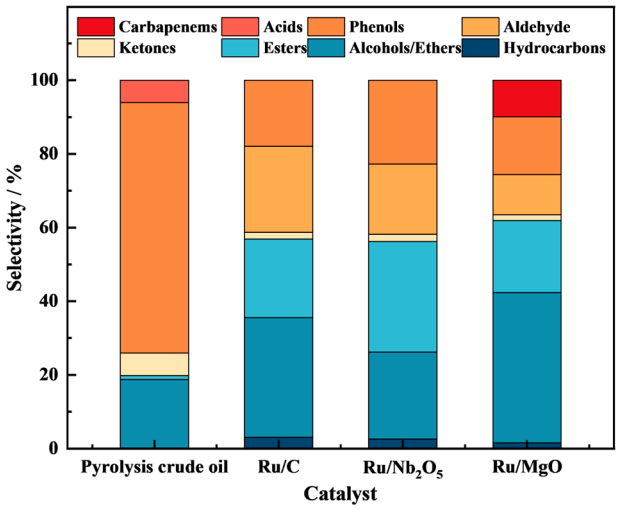

Figure 1. Selectivity of pyrolysis crude oil and upgraded oils from various catalyst supports.

In order to examine the effects of two frequently utilized noble metal catalysts, Ru and Pt, on the quality improvement of pyrolysis crude oil, this paper used Ru/MgO and Pt/MgO as catalysts for experimental investigation, respectively. The main reaction products are shown in Table 4, and all substances and their proportions are shown in Appendix A Table A3. The selectivity and yield of the reaction products are shown in Figure 2. It can be found that both the selectivity (83.3%) and yield (17.8 wt%) of Pt/MgO as a catalyst are significantly higher than those of Ru/MgO; the selectivity and yield of the target compounds were 73.4% and 8.3%, respectively. Specifically analyzing each component, the selectivity of the four target components of hydrocarbons, alcohols/ethers, esters, and ketones in the reaction results of Pt/MgO are all higher than those of Ru/MgO. Existing research has demonstrated that in the process of upgrading pyrolysis oil, Ru as a catalyst tends to produce more solid byproducts compared to Pt [25,45]. This can be attributed to the catalytic properties of Ru, which facilitate carbon–carbon bond formation reactions, leading to the generation of heavier and more polymerized compounds that form solid residues [46,47]. In contrast, Pt catalysts are more effective in hydrodeoxygenation reactions [48], resulting in the breakdown of larger molecules into smaller, more volatile compounds and reducing the formation of solid byproducts. In this study, the mass of solid residue after the reaction with Pt/MgO is 0.3250 g, while the residue from Ru/MgO weighs 0.3526 g, which is consistent with previous findings. This may also be one of the reasons why Pt/MgO exhibits superior performance in our research.

Table 4. Main substances in the GC–MS analysis results of upgraded oil after reaction of various metal catalysts.

Substance	Relative Peak Area (%) *	
	Pt/MgO	Pt–Ni/MgO
Hydrocarbons		
Dodecane	3.27	
Alcohols/Ethers		
Ethane, 1,1-diethoxy-	9.95	7.63
1-Butanol	31.90	23.59
1-Hexanol	3.86	3.75
Ethyl ether	0.90	28.46
Esters		
Ethyl Acetate	11.59	4.18
Butanoic acid, ethyl ester	8.31	0.76
Ketones		
Butanal	1.97	
Cyclopentanone, 2-methyl-		2.09
Aldehyde		
Acetaldehyde	6.02	
2-Butenal	2.06	
Phenols		
Phenol	1.72	3.31
Phenol, 3-methyl-	1.68	5.76
Creosol		1.71
Phenol, 4-ethyl-2-methoxy-		1.64
Phenol, 2-methoxy-4-propyl-		3.06

* The reaction results of Ru/MgO are shown in Table 3.

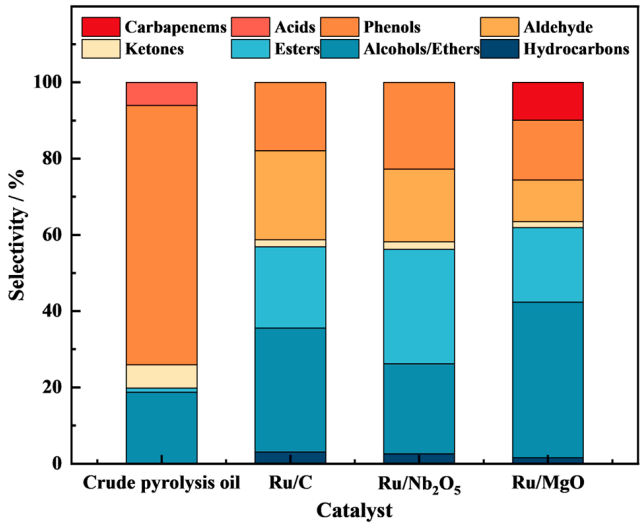

Figure 2. Product selectivity and yield of upgraded oils from various catalyst loading types.

At the same time, this study also carried out bimetallic doping modification research on Pt/MgO, and prepared a Pt–Ni/MgO catalyst. Due to the changes in aggregation and electronic effects, bimetallic catalysts have better catalytic activity than the corresponding single metals [49]. The results of the Pt–Ni/MgO catalytic reaction are shown in Figure 2, and the specific types and amounts of substances can be found in Table A3. It can be found that compared with Pt/MgO catalysis, the yield of target compounds of Pt–Ni/MgO (26.67 wt%) increases significantly. Related research has shown that the existence of Pt promotes the protonation of water and hydrogen, and after spillover from the surface, it enters the Ni center to form in situ acid sites, thereby enhancing the hydrogenation of

the reaction feedstock [50]. At the same time, Pt can prevent the oxidation and leaching of active nickel [51]. Therefore, the synergistic effect of Pt and Ni bimetals leads to the observation of more target compounds in this experiment.

In summary, to further elucidate the catalytic process of Pt–Ni/MgO, phenol was used as an example to illustrate some of the possible reactions occurring on the Pt–Ni/MgO catalyst, as shown in Figure 3. The phenolic hydroxyl group is adsorbed by the basic MgO, protons are transferred, and hydrogen bonds are weakened. At the same time, H_2 is adsorbed on the Pt sites, dissociating into active hydrogen. A portion of the active hydrogen acts on the adsorbed benzene ring, causing phenol to hydrogenate into cyclohexanol and complete desorption. A portion of the active hydrogen enters the Ni center to form in situ acidic sites, thereby promoting the interaction between active H species and the C-O bond, completing the C-O bond cleavage and ultimately achieving dehydration to form cyclohexane.

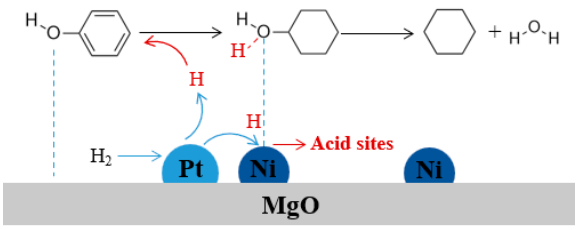

Figure 3. Partial reaction mechanism diagram on Pt–Ni/MgO.

3.3. Catalyst Characterization Results

In this study, we employed a sequential approach to catalyst evaluation and characterization, ensuring that our analysis was both targeted and relevant. Initially, we conducted a comprehensive screening of various catalysts to identify the most effective one for the hydrodeoxygenation reaction. Following this screening, we performed detailed characterization of the best-performing catalyst, Pt–Ni/MgO, to understand the properties that contributed to its superior performance. The characterization results are as follows.

3.3.1. Nitrogen Adsorption–Desorption Isotherms

The pore structure parameters of Pt–Ni/MgO are shown in Table 5. The catalyst has a smaller specific surface area, 26.5653 m^2/g, which is related to the occupation of pores by Ni and Pt. The pore volume and average pore size are larger; 0.2405 cm^3/g and 42.6071 nm, respectively. Related research has shown that there is a direct correlation between pore size and the mass transfer coefficient of the deoxygenation reaction, with larger pores leading to higher coefficients [52]. This is because organic volatiles are able to diffuse more easily through porous media with higher pore sizes and volumes, and these characteristics can withstand more exposed surfaces, enhancing the dispersion of active metals, thereby improving the conversion ability of deoxygenation activity and acidic sites. Figure 4 shows the results of N_2-TPD of the Pt–Ni/MgO catalyst. The catalyst reveals the characteristic type III isotherms with an H3 hysteresis loop [53], and its high-pressure adsorption amount is large, indicating that the Pt–Ni/MgO catalyst is a porous solid with a narrow slit pore structure formed by particle accumulation. According to the pore size distribution, the pores of the Pt–Ni/MgO catalyst are predominantly dispersed in the range of 1–3.5 nm and greater than 40 nm.

Table 5. The pore structure parameters of Pt–Ni/MgO catalysts.

SBET [a] (m^2/g)	Pore Volume [b] (cm^3/g)	Pore Size [c] (nm)
26.5653	0.2405	42.6071

[a] BET method; [b] Calculated using the data from P/P0 = 0.99; [c] BJH method.

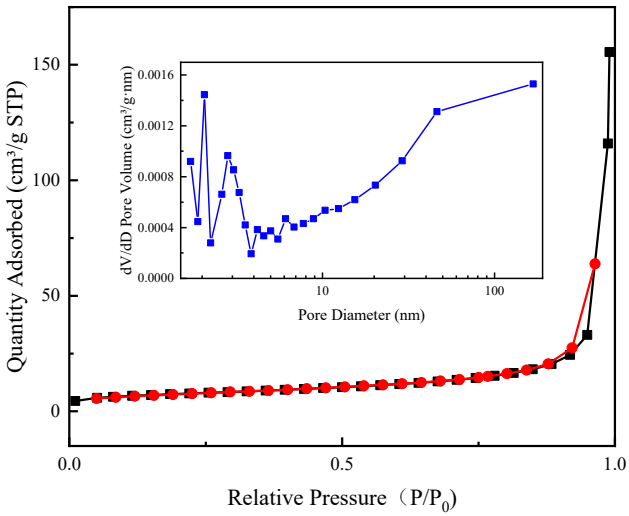

Figure 4. N_2-TPD curve and BJH pore size distribution of Pt–Ni/MgO catalyst.

3.3.2. X-Ray Diffraction (XRD)

The XRD pattern of Pt–Ni/MgO is shown in Figure 5. It is evident that there are five strong diffraction peaks in the spectrum, located at 2θ = 37.032°, 43.035°, 62.429°, 74.817°, and 78.658°, corresponding to the five diffraction planes of MgO: (111), (200), (220), (311), and (222). The grain size calculated using the Debye–Scherrer formula is 34.159 nm. At the same time, the catalyst does not show the diffraction peaks corresponding to the active metals Pt and Ni. It is speculated to result from the good dispersion of the metal across the support surface, and the low loading amount of Pt (2 wt%). Furthermore, a comparative study between the Pt–Ni/MgO and Pt/MgO catalysts found that Pt–Ni/MgO achieved a higher yield of the target compounds, indirectly demonstrating that Ni is effectively dispersed on the catalyst surface, thereby enhancing the overall catalytic activity. Similar findings have been reported in the literature. For example, Xu [54] et al. observed that the absence of characteristic peaks for Pt and Nb in the XRD patterns of Pt/$Nb_xAl_2O_{3.3}$ catalysts was attributed to the good dispersion of these metals on the catalyst surface.

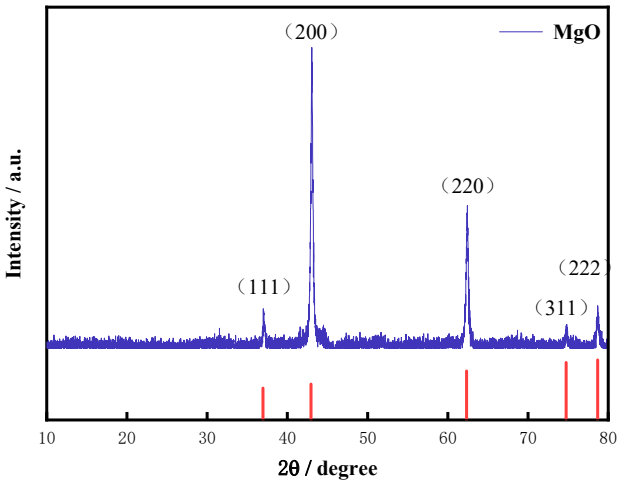

Figure 5. XRD spectrum of Pt–Ni/MgO catalyst.

3.3.3. X-Ray Photoelectron Spectroscopy (XPS)

The XPS spectrum of Pt–Ni/MgO is shown in Figure 6. Figure 6a displays the characteristic peaks of zero-valent Pt metal, Pt 4f5/2 (74.28 eV), and Pt 4f7/2 (71.17 eV) [55], from which it can be inferred that Pt is loaded on the support surface in its metallic form. As shown in Figure 6b, the characteristic peaks of divalent Ni^{2+} Ni 2p1/2 and Ni 2p3/2, as well as the characteristic peaks of zero-valent Ni metal Ni 2p1/2 and Ni 2p3/2 [6,56,57] were found in the spectrum, which is due to the strong interaction between Ni and the MgO support [58]. At the same time, Figure 6c shows the existence of the characteristic peak of divalent Mg^{2+} 1s (1303.27 eV), which can be attributed to MgO [59]. Combined with the XRD test results, it can be deduced that the metals Pt and Ni are present and have good dispersion on the surface of MgO.

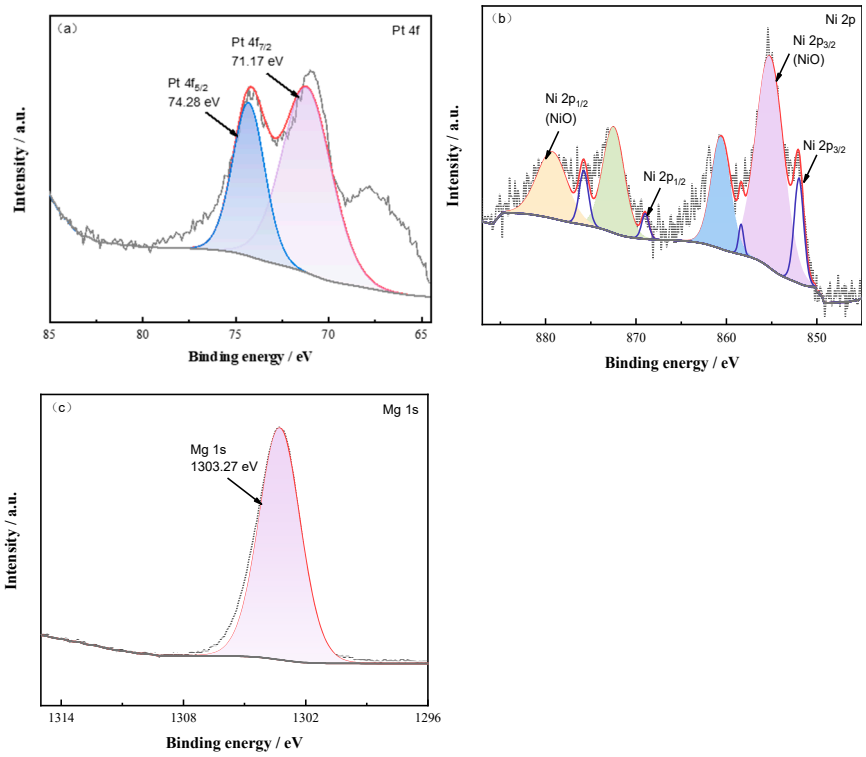

Figure 6. XPS spectrum of Pt–Ni/MgO catalyst: (**a**) Pt; (**b**) Ni; (**c**) Mg.

3.3.4. Scanning Electron Microscopy (SEM)

The SEM characterization results of the Pt–Ni/MgO catalyst are shown in Figure 7. It is evident that the catalyst surface is composed of agglomerates of spherical particles with uniform particle sizes. The particle size is about 50–100 μm, which is moderate in size and is favorable for providing a sufficient active surface area to promote the adsorption–desorption and reaction of raw materials.

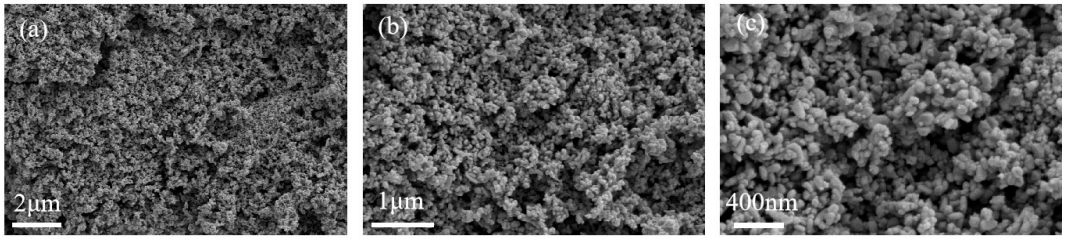

Figure 7. SEM images of Pt–Ni/MgO catalysts: (**a**) 2 μm scale; (**b**) 1 μm scale; (**c**) 400 nm scale.

3.4. The Influence of Reaction Conditions

In an effort to further investigate the factors influencing the efficiency of Pt–Ni/MgO catalyzed directional conversion of pyrolysis crude oil into automotive liquid fuel, this study also examined the impact of temperature on product distribution. Figure 8 illustrates the variation in gas phase components collected after the reaction as a function of temperature. At 250 °C, the primary gas phase components include H_2, CO_2, and CO, along with small amounts of CH_4, C_2H_6, and C_2H_4. As the temperature increases to 270 °C, the quantities of these gases increase, and small amounts of C_3H_6 and C_4H_{10} are detected. At 290 °C, the amount of H_2 slightly increases, while the concentrations of CO, CH_4, C_2H_6, and C_2H_4 significantly increase, with small amounts of C_3H_6, C_4H_{10}, and C_4H_8 also being detected. It can be observed that the yield of H_2 increases significantly with rising temperature. This phenomenon is due to the fact that high temperatures enhance hydrogen production from ethanol reforming. Additionally, the increase in CH_4, C_2H_6, and C_2H_4 at 290 °C is attributed to the higher propensity for C-C and C-H bond cleavage at elevated temperatures, thereby increasing the formation of small hydrocarbon molecules.

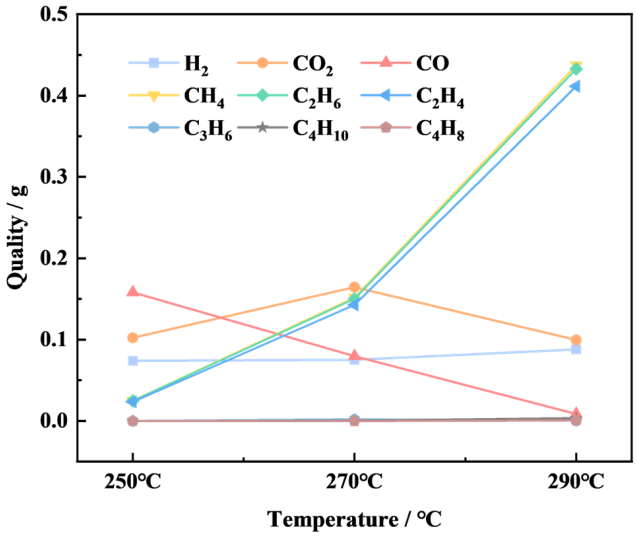

Figure 8. Variation in the quality of gas phase substances with reaction temperature.

The main liquid phase reaction products are shown in Table 6, and all substances and their proportions are shown in Appendix A Table A4. Figure 9 presents the distribution of various substances at three reaction temperatures: 250 °C, 270 °C, and 290 °C. The findings indicate that the production of target compounds increases as the reaction temperature rises. At 270 °C, the catalyst's activity for the hydrodeoxygenation reaction of pyrolysis crude oil is insufficient, yielding only 14.8 wt%. However, at 290 °C, the yield significantly increases to 26.7 wt%, and at this point, the energy conversion rate can reach 72.6%. This phenomenon is attributed to the fact that high temperatures facilitate the cleavage of chemical bonds, while the increased hydrogen production from ethanol reforming creates a hydrogen-rich atmosphere that enhances hydrodeoxygenation activity. Further analysis of the product distribution suggests that high temperatures facilitate the hydrodeoxygenation reaction of phenolic substances, leading to an increase in cyclohexanol and cyclohexanone substances. Simultaneously, the increase in alcohol/ether substances might also be associated with the intensified decomposition of ester substances at high temperature.

Table 6. Main substances in the GC–MS analysis results of upgraded oil after reaction at various temperatures.

Substance	Relative Peak Area (%) *	
	250 °C	270 °C
Alcohols/Ethers		
Ethane, 1,1-diethoxy-	9.71	9.57
1-Butanol	28.83	32.44
Butane, 1,1-diethoxy-	1.71	1.74
1-Hexanol	2.44	4.28
Esters		
Ethyl Acetate	8.72	8.19
Ethyl Oleate	3.95	2.61
Octadecanoic acid, ethyl ester	2.15	2.13
Acetaldehyde	5.35	8.16
Butanal	4.96	4.40
2-Butenal	1.73	1.82
Phenols		
Phenol	2.86	2.29
Phenol, 2-methoxy-	2.08	1.24
Phenol, 2-methyl-	1.72	1.34
Phenol, 3-methyl-	4.21	3.22
Creosol	2.55	1.83
Phenol, 4-ethyl-	1.91	
Phenol, 4-ethyl-2-methoxy-	2.13	1.59
Phenol, 2-methoxy-4-propyl-	3.49	2.26
Homosyringaldehyde	1.59	

* The reaction results at 290 °C are shown in Table 4 of Pt–Ni/MgO.

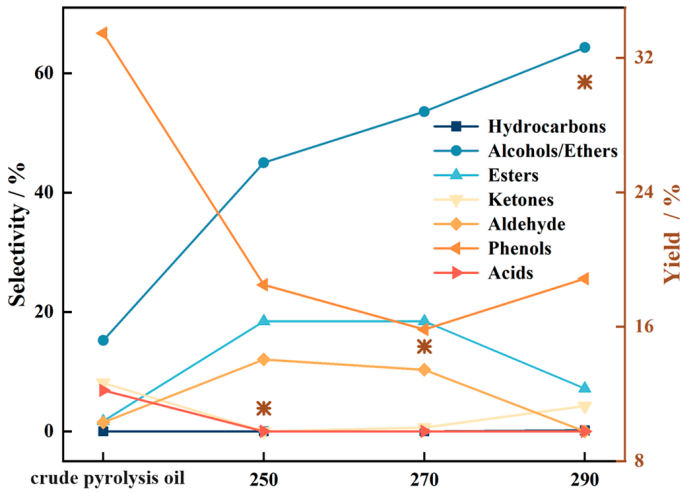

Figure 9. Liquid phase product selectivity and yield of various temperatures.

Further analysis was conducted on the composition of the pyrolysis crude oil before and after the reaction at 290 °C. It is first noted that the acids in the raw material are completely transformed, which significantly improved the pH value of the liquid. To further explain this phenomenon, acetic acid was chosen as the model compound to carry out hydrodeoxygenation experiments under the same reaction conditions. The results indicate that acetic acid undergoes complete conversion, primarily due to the ethanol present in quantities far exceeding what is required for the esterification reaction. In addition, the supercritical state produced in this study can accelerate the esterification of acetic acid. Li et al. [60] demonstrated that acetic acid could be completely converted even without a catalyst under the supercritical state of methanol. The main reaction pathway of

acetic acid is to undergo esterification with ethanol to obtain ethyl acetate. Furthermore, a minor quantity of butyl acetate is also generated in the reaction. The speculated reaction pathway is that ethanol undergoes dehydrogenation to produce acetaldehyde, acetaldehyde undergoes dehydration condensation to produce (E)-but-2-enal, further hydrogenation to obtain n-butanol, and then esterification with acetic acid to obtain butyl acetate, as shown in Figure 10. In the reaction products of actual bio-oil, a higher content of ethyl acetate and butyl acetate was also detected, which is consistent with the reaction results when acetic acid was used as the model compound.

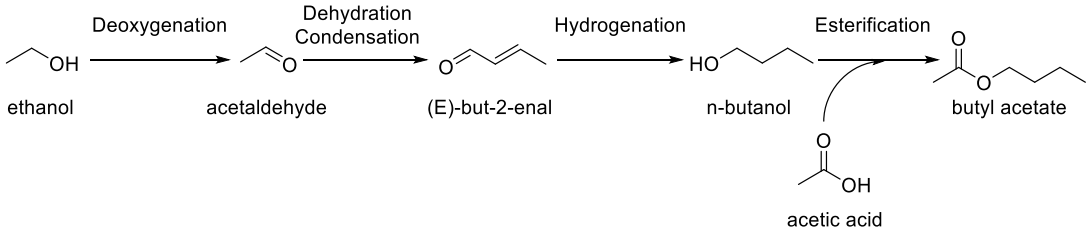

Figure 10. Generation pathway diagram of butyl acetate.

It is also observed that there is a certain degree of reduction in the ketones. To further clarify the reaction process and products of ketones, 1-Hydroxypropan-2-one, which is present in high concentrations in pyrolysis crude oil, was used as a model compound for experimental research. The results show that 1-Hydroxypropan-2-one is quite reactive and undergoes complete conversion, producing various products including ketones and alcohols, as shown in Table 7. This indicates that the carbonyl group (C=O) of the ketone is reduced to -OH by the action of activated hydrogen. This is consistent with the increase in alcohols/ethers observed in the actual pyrolysis oil after the reaction.

Table 7. GC–MS analysis results of the reaction products derived from 1-Hydroxypropan-2-one.

Substance Name	Relative Peak Area (%)
2-Butanol, 1-methoxy-	29.80
3-Pentanol, 2,4-dimethyl-	14.87
Propane, 2-ethoxy-	10.88
2,3-Butanediol	9.28
2-Hexanol, 2,3-dimethyl-	7.62
1,3-Dioxane, 2-methyl-	7.45
3-Hydroxy-2-butanone	6.32
3-Hexanol, 4-methyl-	5.37
2-Hydroxy-3-pentanone	4.44
3-Hexanol, 2-methyl-	3.98

Among various products, the primary ketone substance is 3-Hydroxy-2-butanone. Scholars like Paul et al. [61] suggested that 3-Hydroxy-2-butanone could be converted from pyruvate, which was an important intermediate product formed during the reaction process of 1-Hydroxypropan-2-one. The alcohol substances include 2,3-butanediol and 3-hexanol, 4-methyl-, etc. Furthermore, 2,3-butanediol can be obtained by hydrogenating 3-Hydroxy-2-butanone. At the same time, ketone substances are prone to addition reactions with hydroxyl groups to produce alcohol substances. Therefore, the actual reaction is more complex and requires further in-depth research.

Moreover, the detection of hydrocarbons in the reaction products indicates that the Pt–Ni/MgO catalyst exhibits good hydrodeoxygenation activity at 290 °C. Additionally, the processes of cellulose and hemicellulose dehydration cyclization, as well as lignin cracking, produce aldehydes. These substances are prone to undergoing self-polymerization or

condensation reactions with phenols, impacting the stability of the oil product. Therefore, in this research, furfural was chosen as the model compound to verify the reaction system's effectiveness on aldehydes. Based on the analysis in this paper and the relevant literature [42,62–64], the main conversion pathways of furfural are illustrated in Figure 11, with the substances in red being the components detected in this study. These pathways likely involve hydrogenation, decarbonylation, and other reactions that can convert furfural into less reactive and more stable molecules, thereby enhancing the stability of the bio-oil.

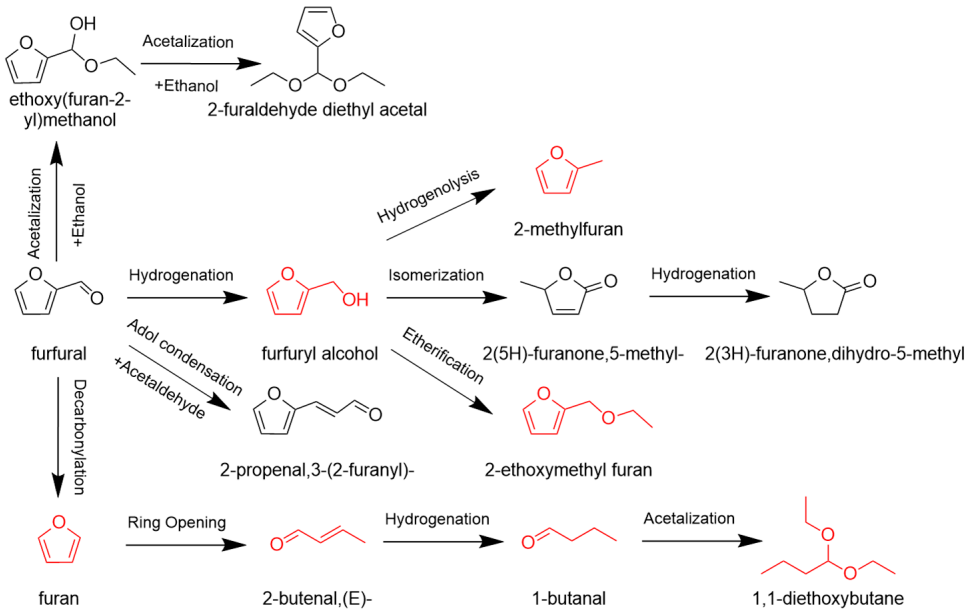

Figure 11. Main conversion pathways of furfural.

The products of the furfural reaction are shown in Table 8, and it can be inferred that the existing reaction pathways include: (1) Hydrogenation to produce furfuryl alcohol, which reacts with ethanol to produce 2-ethoxymethyl furan through etherification; (2) Furfuryl alcohol produced by hydrogenation of furfural further undergoes hydrodeoxygenation to produce 2-methylfuran; (3) At higher temperatures, furan is produced through decarbonylation, which further undergoes ring-opening, hydrogenation, and aldol condensation to produce 1,1-diethoxybutane. It can be observed that in this study, hydrogenation–etherification is the primary reaction route for furfural, and the selectivity of furfuryl alcohol to 2-ethoxymethyl furan is higher than that of 2-methylfuran. This indicates that the significant presence of ethanol makes furfuryl alcohol more inclined to undergo etherification.

Table 8. GC–MS analysis results of the reaction products derived from furfural.

Substance Name	Relative Peak Area (%)
2-ethoxymethyl furan	24.85
furfuryl alcohol	16.44
2-methylfuran	13.98
2-butenal, (E)-	10.64
1,1-diethoxybutane	10.03
1-butanal	8.36
furan	3.81

In summary, it can be concluded that at 290 °C, there is effective conversion of acids, ketones, and aldehydes, which facilitates the production of stable and combustible liquid fuel components. To deepen the understanding of hydrodeoxygenation of biomass pyrolysis oil, a comparative analysis was conducted between our experimental results and those

reported in the contemporary literature. The comparative data are summarized in Table 9, which includes reaction conditions, catalysts, selectivity, and yield. It can be observed that the selectivity of the target compounds in this study is 75.8%, whereas in concurrent studies, this figure typically ranges from 13.0% to 71.4%. Current research on yield is relatively scarce, with only one study reporting a yield of 3.9 mg/mL, while in this study, the yield is 26.7 mg/mL. This indicates a significant improvement in the reaction effect in this study. Additionally, it can be noted that the reaction conditions used in this study are relatively mild, further validating the feasibility and advancement of the research.

Table 9. Comparative study on the preparation of liquid fuels from pyrolysis crude oil.

Conditions	Catalysts	Selectivity	Yield	Reference
290 °C, 0.50 Mpa H_2	Pt–Ni/MgO	75.8%	26.7 mg/mg	This paper
300 °C, 3 Mpa H_2	Pt/C	13.0% *	3.9 mg/mL	[25]
300 °C, 0.34 MPa N_2	Zn	69.0%	-	[65]
350 °C, 3.45 MPa H_2	Ni/AC	39.4%	-	[66]
200 °C, 2.07 MPa H_2	Pd/C, $ZnCl_2$	71.4%	-	[67]

* The experimental data were obtained from the heavy oil collected after the reaction.

3.5. The Physicochemical Properties of Pyrolysis Crude Oil and Upgrading

FT-IR analysis was further carried out to verify the changes in pyrolysis crude oil and upgraded oil. The peak assignments and peak areas are presented in Table 10, and the FT-IR spectrum is presented in Figure 12. It is readily apparent that after the hydrodeoxygenation reaction, several peaks in the spectrum disappeared compared to those of the pyrolysis crude oil. Specifically, the peak at 1514 cm^{-1} can be attributed to the vibration of the aromatic ring, while the peak at 1272 cm^{-1}, with an area of 430, can be assigned to the C-O stretching vibration or C-O-C symmetric stretching vibration. The disappearance of these two peaks indicates a reduction in the unsaturation and oxygen content of the upgraded oil, thereby improving its stability. Simultaneously, a peak at 2880 cm^{-1}, with an area of 246, was found in the upgraded oil, which is attributed to the C-H in the methoxy group. This phenomenon is consistent with the increase in alcohols/ethers after the reaction of pyrolysis crude oil.

Additionally, the strong absorption at 3341 and 3322 cm^{-1} is caused by H_2O. The peaks at 1656 and 1642 cm^{-1} are due to the stretching of C=C, and it can be observed that the peak area in the upgraded oil is 300, which is 25.32% of the 1185 area in the pyrolysis crude oil, indicating a significant reduction in peak intensity. This further proves that the upgraded oil underwent hydrogenation reactions, leading to a decrease in unsaturation. The peaks at 1087 and 1085 cm^{-1} belong to the C-O deformation in secondary alcohols and aliphatic ethers, with the peak area increasing from 185 in the pyrolysis crude oil to 476 in the upgraded oil. The characteristic peaks at 2976 and 2973 cm^{-1} are attributed to the C-H in aliphatic and aromatic groups, with the peak area in the upgraded oil being 2.21 times that of the pyrolysis crude oil, indicating effective hydrogenation in the upgraded oil. The characteristic peaks at 879 and 877 cm^{-1} are due to the C-H deformation of aromatic in-plane and C-O deformation of primary alcohols, with the peak area increasing from 150 in the pyrolysis crude oil to 560 in the upgraded oil. This demonstrates that aromatic compounds underwent effective hydrogenation, and the content of alcohols increases after the reaction. Other characteristic peaks include 1381 and 1379 cm^{-1} (O-H in-plane bending and C-H bending) and 1046 and 1044 cm^{-1} (C-O stretching vibration).

Table 10. Peaks assignments of FT-IR spectra.

Source	Wavenumber (cm^{-1})	Assignments	Peak Areas
Pyrolysis crude oil	3341	H_2O	13,053
Refined oil	3322	H_2O	8380
Pyrolysis crude oil	2976	C–H in aliphatic and aromatic groups	168
Refined oil	2973	C–H in aliphatic and aromatic groups	371
Refined oil	2880	C–H in methoxy group	246
Refined oil	1656	C=C stretching	300
Pyrolysis crude oil	1642	C=C stretching	1185
Pyrolysis crude oil	1514	Aromatic ring vibration	86
Pyrolysis crude oil	1381	O–H in-plane bending and C–H bending	52
Refined oil	1379	O–H in-plane bending and C–H bending	67
Pyrolysis crude oil	1272	C-O stretching vibration or C-O-C symmetric stretching vibration	430
Refined oil	1087	C-O deformation in secondary alcohols and aliphatic ethers	476
Pyrolysis crude oil	1085	C-O deformation in secondary alcohols and aliphatic ethers	185
Refined oil	1046	C-O stretching vibration	1136
Pyrolysis crude oil	1044	C-O stretching vibration	918
Refined oil	879	C–H deformation of aromatic in-plane and C-O deformation of primary alcohols	560
Pyrolysis crude oil	877	C–H deformation of aromatic in-plane and C-O deformation of primary alcohols	150

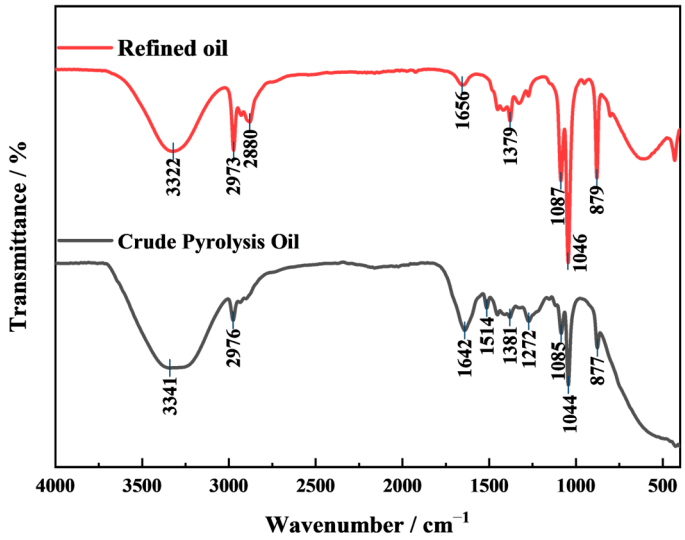

Figure 12. FT-IR spectrum of pyrolysis crude oil and upgraded oil.

The fundamental physicochemical properties of pyrolysis crude oil, upgraded oil, ethanol, and bio-diesel are presented in Table 11 [68,69]. It is observed that, compared to pyrolysis crude oil, upgraded oil exhibits a lower density (0.82 g/mL at 20 °C) and viscosity (1.11 cSt at 40 °C). This indicates that some of the larger molecular substances in the pyrolysis crude oil have been transformed into smaller organic molecules, significantly enhancing the practicality of the upgraded oil. Additionally, due to the high content of carboxylic acids in the pyrolysis crude oil, its pH value is relatively low at 3.8, while the pH value of the upgraded oil has significantly improved to 6.0, which greatly enhances the practicality of the oil. Furthermore, the calorific value of the upgraded oil can reach 28.9 kJ/g, which aids in improving engine efficiency and reducing the costs associated with the transportation and storage of the fuel. When comparing upgraded oil with ethanol

and biodiesel, its density, viscosity, and calorific value are found to be similar to those of ethanol, suggesting that upgraded oil is a potential substitute or additive for existing fossil fuels.

Table 11. Basic properties of pyrolysis crude oil, upgraded oil (removing water), ethanol, and bio-diesel.

	Pyrolysis Crude Oil	Upgraded Oil	Ethanol	Bio-Diesel
Density (g/mL, 20 °C)	0.98	0.82	0.79	0.86–0.9
Kinematic viscosity (cSt, 40 °C)	2.01	1.11	1.2	1.9–6.0
pH	3.8	6.0	7	-

3.6. Reproducibility Verification

Due to limitations in resources and time, we were unable to conduct extensive reproducibility tests within the scope of this study. Therefore, we selected the optimal experimental conditions from the study, specifically using the Pt–Ni/MgO catalyst at a temperature of 290 °C, to perform repeated experiments to verify the repeatability of the data. The selectivity of the products obtained from three independent experiments under these conditions is shown in Table 12. The data indicate that the standard error of the metrics is within 0.8. Except for hydrocarbons and carbapenems, which have a relative standard error exceeding 10% due to their inherently low selectivity, the relative standard error for other substances is less than 7%. Notably, the relative standard error for the target compounds is 0.41%, demonstrating good reproducibility of the experimental data.

Table 12. Reproducibility analysis of product selectivity.

	1st	2nd	3rd	Average	Standard Error	Relative Standard Error
Hydrocarbons	0.5	0.3	0.5	0.43	0.07	16.26%
Alcohols/Ethers	56.2	53.7	53.9	54.60	0.79	1.45%
Esters	15.5	17.6	18.1	17.07	0.77	4.50%
Ketones	0.8	1.0	0.9	0.90	0.06	6.67%
Aldehyde	18.9	19.2	19.6	19.23	0.21	1.10%
Phenols	5.4	6.0	5.1	5.50	0.26	4.73%
Carbapenems	2.8	2.3	1.8	2.30	0.29	12.61%
Target compounds	75.8	74.9	74.8	75.17	0.31	0.41%

3.7. Economic Analysis of Liquid Fuel Production

Economic feasibility analysis is crucial for the further development and commercial application of the technological route. In this study, the raw material costs for producing each ton of fuel are shown in Table 13. The quantities of raw materials are based on actual research results, and the costs of the raw materials are referenced from the relevant literature and major shopping websites [65,70]. It can be observed that the catalyst is the primary cost source in this process route. Therefore, in subsequent research, further improving the process to increase the yield of liquid fuel and reduce catalyst coking and deactivation is an important research direction. In this study, the price of liquid fuel is $1838.32/t, while the current price of automotive fuel ranges from $1211.03/t to $2029.75/t, indicating that this study has a certain degree of economic feasibility. It should be noted that these data are based on current market conditions and reference materials, and there may be some

fluctuations. Considering the use of government subsidies or carbon reduction credits, the cost is expected to be further reduced.

Table 13. The raw material costs for producing each ton of fuel.

Item	Unit Price ($/t)	Quantity (kg)	Total Price ($)
Cotton stalks	34.80	2697.11	93.86
Catalyst	502,007.34	3.40	1705.53
Industrial water	0.67	1885.97	1.26
H_2	3549.14	10.62	37.68
Total			1838.33

4. Conclusions

This study conducted an exploration of the reaction pathways of pyrolysis crude oil model compounds in a high-pressure solvothermal reaction kettle, while also undertaking experimental research on the solvothermal directional conversion of actual pyrolysis crude oil under different catalysts and reaction temperatures. The feasibility of producing automotive liquid fuel from pyrolysis crude oil under mild reaction conditions was confirmed.

The results showed that among the neutral, acidic, and alkaline supports loaded with Ru, the alkaline MgO achieved the highest selectivity of target compounds, reaching 73.4%. Moreover, the alkaline catalyst support was more inclined to generate alcohol/ether substances. Simultaneously, the hydrodeoxygenation activity of the bimetallic catalyst Pt–Ni/MgO was greater than that of the single metal Pt/MgO and the single metal Ru/MgO. At the optimal reaction temperature of 290 °C, the yield of target compounds of liquid fuel could reach 26.7 wt%, the energy conversion rate could reach 72.6%, and the selectivity could reach 75.8%, exceeding the results of concurrent studies (13.0–71.4%). At the same time, the density, kinematic viscosity, pH value, and calorific value of the upgraded oil are all similar to those of ethanol, indicating that the upgraded product is a potential substitute or additive for existing fossil fuels. Under these reaction conditions, pyrolysis crude oil model compounds such as acetic acid, furfural, and 1-Hydroxypropan-2-one could achieve 100% conversion.

Phenols and their oligomers, as the challenging points in the conversion of pyrolysis crude oil, still have potential for further optimization. Related studies have shown that acidic conditions will enhance cracking and oxygen removal, which are beneficial for further improving the activity of phenol conversion. In-depth research on the conversion of phenols and the optimization of reaction conditions (pressure, ethanol/bio-oil ratio, time) will be conducted in the future.

Author Contributions: Conceptualization, Q.W. and Z.L.; Data curation, Q.Q.; Formal analysis, Q.W.; Funding acquisition, Z.L.; Investigation, Q.W. and J.S.; Methodology, Q.W.; Supervision, Z.L. and F.M.; Validation, Q.Q. and F.M.; Visualization, J.S.; Writing—original draft, Q.W.; Writing—review & editing, Z.L. All authors have read and agreed to the published version of the manuscript.

Funding: This research was funded by National Key Research and Development Program of China, grant number 2023YFE0111600.

Data Availability Statement: The data presented in this study are available on request from the corresponding author. The data are not publicly available due to privacy restrictions.

Conflicts of Interest: The authors declare no conflicts of interest.

Abbreviations

The following abbreviations are used in this manuscript:

FT-IR	Fourier Transform Infrared Spectroscopy
GC–MS	Gas Chromatography coupled with Mass Spectrometry
GPC	Gel Permeation Chromatography
LMW	Low Molecular Weight
XPS	X-Ray Photoelectron Spectroscopy
HMW	High Molecular Weight
SEM	Scanning Electron Microscope
XRD	X-Ray Diffraction

Appendix A

Table A1. GC–MS analysis results of pyrolysis crude oil.

Substance Type	Substance Name	Relative Peak Area (%)
Alcohols/Ethers	Ethanol	16.59
	Melezitose	2.17
Esters	Ethyl Acetate	1.03
Ketones	1-Hydroxypropan-2-one	0.70
	2-Cyclopenten-1-one, 2-methyl-	1.18
	2-Cyclopenten-1-one, 3-methyl-	1.28
	1,2-Cyclopentanedione, 3-methyl-	2.95
Phenols	Phenol	4.91
	Phenol, 2-methoxy-	4.46
	Phenol, 2-methyl-	3.02
	Phenol, 3-methyl-	6.00
	Creosol	3.53
	Phenol, 2,6-dimethyl-	2.28
	Phenol, 3,4-dimethyl-	1.08
	Phenol, 4-ethyl-	2.05
	Phenol, 3-ethyl-	1.07
	Phenol, 4-ethyl-2-methoxy-	2.02
	Phenol, 2-ethyl-5-methyl-	0.94
	Phenol, 2-propyl-	0.81
	p-Cymen-7-ol	1.18
	Phenol, 2-methoxy-3-(2-propenyl)-	1.75
	Phenol, 2-methoxy-4-propyl-	0.74
	Catechol	6.17
	Phenol, 2,6-dimethoxy-	3.90
	Phenol, 2-methoxy-4-(1-propenyl)-, (Z)-	1.56
	1,2-Benzenediol, 4-methyl-	4.65
	trans-Isoeugenol	3.25
	3,5-Dimethoxy-4-hydroxytoluene	2.15
	Vanillin	1.81
	4-Ethylcatechol	2.36
	5-tert-Butylpyrogallol	1.24
	Apocynin	1.92
	2-Propanone, 1-(4-hydroxy-3-methoxyphenyl)-	0.98
	Phenol, 2,6-dimethoxy-4-(2-propenyl)-	1.09
	(E)-2,6-Dimethoxy-4-(prop-1-en-1-yl)phenol	1.14
Acids	Acetic acid	6.04

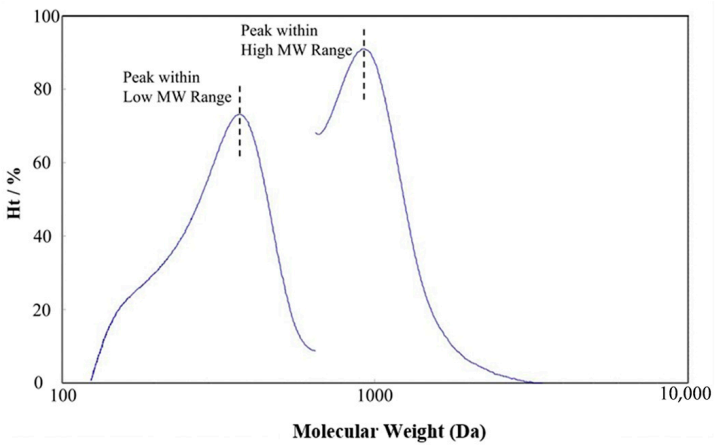

Figure A1. Molecular weight distribution of pyrolysis crude oil.

Table A2. GC–MS analysis results of upgraded oil after reaction of various catalyst supports.

Catalyst	Substance Type	Substance Name	Relative Peak Area (%)
Ru/C	Hydrocarbons	Butane	0.31
		Heptane	0.77
		Octane	0.90
		Nonane	1.08
	Alcohols/Ethers	1-Butanol	22.18
		Ethyl ether	2.74
		Isopropyl Alcohol	0.96
		1-Propanol	0.71
		Ethane, 1,1-diethoxy-	4.42
		1,2-propanediol	0.44
		Cyclopentanol, 2-methyl-	1.08
	Esters	Ethyl Acetate	18.90
		Butanoic acid, ethyl ester	1.60
		Pentanoic acid, ethyl ester	0.78
	Ketones	Cyclopentanone, 2-methyl-	1.16
		Cyclopentanone, 2-ethyl-	0.68
	Aldehyde	Acetaldehyde	23.30
	Phenols	Phenol	2.25
		Phenol, 2-methoxy-	2.10
		Phenol, 2-methyl-	1.58
		p-Cresol	1.16
		Phenol, 3-methyl-	1.79
		Creosol	1.85
		Phenol, 2,4-dimethyl-	0.83
		Phenol, 4-ethyl-	0.52
		Phenol, 4-ethyl-2-methoxy-	2.55
		Phenol, 2-methoxy-4-propyl-	3.39
Ru/Nb_2O_5	Hydrocarbons	Butane	0.39
		Heptane	0.74
		Octane	0.68
		Nonane	0.81
	Alcohols/Ethers	Ethyl ether	3.79
		Propane-1,3-diol, 2-methyl-	0.95
		Ethane, 1,1-diethoxy-	8.37
		1-Butanol	10.44

Table A2. *Cont.*

Catalyst	Substance Type	Substance Name	Relative Peak Area (%)
	Esters	Ethyl Acetate	27.37
		Butanoic acid, ethyl ester	1.67
		Pentanoic acid, ethyl ester	0.99
	Ketones	Cyclopentanone, 2-methyl-	1.25
		Cyclopentanone, 2-ethyl-	0.74
	Aldehyde	Acetaldehyde	14.09
		Propanal, 2-methyl-	4.94
	Phenols	Phenol	2.78
		Phenol, 2-methoxy-	0.61
		Phenol, 2-methyl-	1.70
		Phenol, 2-ethoxy-	1.51
		Phenol, 3-methyl-	1.45
		p-Cresol	1.42
		Creosol	0.94
		Phenol, 2-ethyl-	0.65
		Phenol, 2,4-dimethyl-	0.92
		2-Ethoxy-4-methylphenol	3.60
		Phenol, 4-ethyl-	0.78
		Phenol, 4-ethyl-2-methoxy-	0.85
		Benzene, 1-ethoxy-2-methoxy-4-methyl-	2.56
		Phenol, 2-methoxy-4-propyl-	1.16
		t-Butylhydroquinone	0.98
		Resorcinol, 4-pentyl-	0.85
Ru/MgO	Hydrocarbons	Dodecane	1.57
	Alcohols/Ethers	Furan, 2,5-dihydro-	5.00
		Ethane, 1,1-diethoxy-	12.30
		1-Butanol	23.96
		Crotonyl alcohol	4.92
		Butane, 1,1-diethoxy-	1.26
		1-Hexanol	1.56
		Hexane, 1-(1-ethoxyethoxy)-	0.99
		3-(1-Ethoxy-ethoxy)-butan-1-ol	0.72
	Esters	Ethyl Acetate	13.56
		Propanoic acid, ethyl ester	1.35
		Butanoic acid, ethyl ester	2.19
		Butyl acetate	2.45
	Ketones	Butanal	1.56
	Aldehyde	Acetaldehyde	10.90
	Phenols	Phenol	3.15
		Phenol, 2-methoxy-	0.95
		Phenol, 2-methyl-	1.79
		Phenol, 3-methyl-	3.86
		Creosol	0.89
		Phenol, 3-ethyl-	0.99
		Phenol, 2,6-dimethyl-	1.31
		Phenol, 4-ethyl-	1.54
		Phenol, 2-methoxy-4-propyl-	1.23

Table A3. GC–MS analysis results of upgraded oil after reaction of various metal catalysts.

Catalyst *	Substance Type	Substance Name	Relative Peak Area (%)
Pt–Ni/MgO	Hydrocarbons	Naphthalene	0.15
	Alcohols/Ethers	Ethyl ether	28.46
		Ethane, 1,1-diethoxy-	7.63
		1-Butanol	23.59
		1-Hexanol	3.75
	Esters	Ethyl Acetate	4.18
		Propanoic acid, ethyl ester	0.77
		Butanoic acid, ethyl ester	0.76
		Octadecanoic acid, ethyl ester	1.33
	Ketones	2-Butanone	0.39
		2-Pentanone	0.28
		Cyclopentanone	0.43
		Cyclopentanone, 2-methyl-	2.09
		Cyclopentanone, 2-ethyl-	0.98
	Phenols	Phenol	3.31
		Phenol, 2-methoxy-	1.32
		Phenol, 3-methyl-	5.76
		Phenol, 2,6-dimethyl-	0.25
		Creosol	1.71
		Phenol, 2,4-dimethyl-	1.41
		Phenol, 2,3-dimethyl-	0.70
		Phenol, 4-ethyl-	1.44
		Phenol, 3-ethyl-	1.14
		Benzaldehyde, 3-[4-(1,1-dimethylethyl)phenoxy]-	0.38
		Phenol, 3-ethyl-5-methyl-	0.26
		Phenol, 4-ethyl-2-methoxy-	1.64
		Phenol, 3-ethyl-5-methyl-	0.45
		Phenol, 4-propyl-	1.17
		Phenol, 4-(1-methylpropyl)-	0.65
		1H-Inden-5-ol, 2,3-dihydro-	0.55
Pt/MgO	Hydrocarbons	4-Decene	0.51
		Dodecane	3.27
	Alcohols/Ethers	Ethyl ether	0.90
		Ethane, 1,1-diethoxy-	9.95
		1-Butanol	31.90
		2-Buten-1-ol	0.60
		Propane, 1-(1-methylethoxy)-	0.73
		Butane, 1,1-diethoxy-	1.21
		1-Butanol, 2-ethyl-	1.31
		Butane, 1-(1-ethoxyethoxy)-	0.64
		1-Hexanol	3.86
	Esters	Ethyl Acetate	11.59
		Propanoic acid, ethyl ester	0.70
		Butanoic acid, ethyl ester	8.31
		Pentanoic acid, ethyl ester	1.09
		Hexanoic acid, ethyl ester	1.35
		Octadecanoic acid, ethyl ester	1.39
	Ketones	Butanal	1.97
		Cyclopentanone, 2-ethyl-	0.63

Table A3. *Cont.*

Catalyst *	Substance Type	Substance Name	Relative Peak Area (%)
		Cyclohexanone, 2,6-dimethyl-	0.41
	Aldehyde	Acetaldehyde	6.02
		2-Butenal	2.06
	Phenols	Phenol	1.72
		Phenol, 2-methoxy-	0.50
		Phenol, 2-methyl-	1.01
		Phenol, 3-methyl-	1.68
		Phenol, 2-ethyl-	1.11
		Phenol, 2,6-dimethyl-	0.69
		Phenol, 4-ethyl-	1.03
		Phenol, 2-methoxy-4-propyl-	0.93

* The reaction results of Ru/MgO are shown in Table A2.

Table A4. GC–MS analysis results of upgraded oil after reaction at various temperatures.

Temperature *	Substance Type	Substance Name	Relative Peak Area (%)
250	Alcohols/Ethers	Ethane, 1,1-diethoxy-	9.71
		1-Butanol	28.83
		Cyclopentanol, 2-methyl-	1.07
		Propane, 1-(1-methylethoxy)-	1.26
		Butane, 1,1-diethoxy-	1.71
		1-Hexanol	2.44
	Esters	Ethyl Acetate	8.72
		Butanoic acid, ethyl ester	1.30
		Pentanoic acid, ethyl ester	1.01
		Hexadecanoic acid, ethyl ester	1.28
		Ethyl Oleate	3.95
		Octadecanoic acid, ethyl ester	2.15
	Aldehyde	Acetaldehyde	5.35
		Butanal	4.96
		2-Butenal	1.73
	Phenols	Phenol	2.86
		Phenol, 2-methoxy-	2.08
		Phenol, 2-methyl-	1.72
		Phenol, 3-methyl-	4.21
		Creosol	2.55
		Phenol, 2,5-dimethyl-	1.24
		Phenol, 4-ethyl-	1.91
		Phenol, 4-ethyl-2-methoxy-	2.13
		Phenol, 2-methoxy-4-propyl-	3.49
		5-tert-Butylpyrogallol	0.76
		Homosyringaldehyde	1.59
270	Alcohols/Ethers	Ethyl ether	0.69
		Ethane, 1,1-diethoxy-	9.57
		1-Butanol	32.44

Table A4. *Cont.*

Temperature *	Substance Type	Substance Name	Relative Peak Area (%)
		Propane, 1-(1-methylethoxy)-	0.75
		Butane, 1,1-diethoxy-	1.74
		1-Butanol, 2-ethyl-	1.22
		1-Hexanol	4.28
	Esters	Ethyl Acetate	8.19
		Propanoic acid, ethyl ester	0.75
		Butanoic acid, ethyl ester	1.55
		Pentanoic acid, ethyl ester	1.15
		Hexadecanoic acid, ethyl ester	1.06
		Ethyl Oleate	2.61
		Octadecanoic acid, ethyl ester	2.13
	Ketones	Cyclopentanone, 2-ethyl-	0.60
	Aldehyde	Acetaldehyde	8.16
		Butanal	4.40
		2-Butenal	1.82
		Hexanal	0.74
	Phenols	Phenol	2.29
		Phenol, 2-methoxy-	1.24
		Phenol, 2-methyl-	1.34
		Phenol, 3-methyl-	3.22
		Creosol	1.83
		Phenol, 2,5-dimethyl-	0.97
		Phenol, 3-ethyl-	1.41
		Phenol, 4-ethyl-2-methoxy-	1.59
		Phenol, 2-methoxy-4-propyl-	2.26

* The reaction results at 290 °C are shown in Table A2 of Pt–Ni/MgO.

References

1. Landrat, M.; Abawalo, M.T.; Pikoń, K.; Turczyn, R. Bio-Oil Derived from Teff Husk via Slow Pyrolysis Process in Fixed Bed Reactor and Its Characterization. *Energies* **2022**, *15*, 9605. [CrossRef]
2. Ahmed, G.; Kishore, N. Synergistic Effects on Properties of Biofuel and Biochar Produced through Co-Feed Pyrolysis of Erythrina Indica and Azadirachta Indica Biomass. *Renew. Energy* **2024**, *227*, 120508. [CrossRef]
3. Jerzak, W.; Acha, E.; Li, B. Comprehensive Review of Biomass Pyrolysis: Conventional and Advanced Technologies, Reactor Designs, Product Compositions and Yields, and Techno-Economic Analysis. *Energies* **2024**, *17*, 5082. [CrossRef]
4. Kim, J.-H.; Jung, S.; Lin, K.-Y.A.; Rinklebe, J.; Kwon, E.E. Comparative Study on Carbon Dioxide-Cofed Catalytic Pyrolysis of Grass and Woody Biomass. *Bioresour. Technol.* **2021**, *323*, 124633. [CrossRef]
5. Fernández, I.; Pérez, S.F.; Fernández-Ferreras, J.; Llano, T. Microwave-Assisted Pyrolysis of Forest Biomass. *Energies* **2024**, *17*, 4852. [CrossRef]
6. He, C.; Ruan, T.; Ouyang, X.; Ma, Y.; Qian, Y.; Qiu, X. Selective Hydrodeoxygenation of Monophenolics from Lignin Bio-Oil for Preparing Cyclohexanol and Its Derivatives over Ni-Co/Al_2O_3-MgO Catalyst. *Ind. Crops Prod.* **2023**, *202*, 117045. [CrossRef]
7. Dong, R.; Tang, Z.; Song, H.; Chen, Y.; Wang, X.; Yang, H.; Chen, H. Co-Pyrolysis of Vineyards Biomass Waste and Plastic Waste: Thermal Behavior, Pyrolytic Characteristic, Kinetics, and Thermodynamics Analysis. *J. Anal. Appl. Pyrolysis* **2024**, *179*, 106506. [CrossRef]
8. Wang, T.; Zhou, T.; Li, C.; Song, Q.; Zhang, M.; Yang, H. Development Status and Prospects of Biomass Energy in China. *Energies* **2024**, *17*, 4484. [CrossRef]
9. Reza, M.; Iskakova, Z.; Afroze, S.; Kuterbekov, K.; Kabyshev, A.; Bekmyrza, K.; Kubenova, M.; Bakar, M.; Azad, A.; Roy, H.; et al. Influence of Catalyst on the Yield and Quality of Bio-Oil for the Catalytic Pyrolysis of Biomass: A Comprehensive Review. *Energies* **2023**, *16*, 5547. [CrossRef]

10. Miao, F.; Luo, Z.; Zhou, Q.; Du, L.; Zhu, W.; Wang, K.; Zhou, J. Study on the Reaction Mechanism of C8+ Aliphatic Hydrocarbons Obtained Directly from Biomass by Hydropyrolysis Vapor Upgrading. *Chem. Eng. J.* **2023**, *464*, 142639. [CrossRef]
11. Li, X.; Dong, W.; Zhang, J.; Shao, S.; Cai, Y. Preparation of Bio-Oil Derived from Catalytic Upgrading of Biomass Vacuum Pyrolysis Vapor over Metal-Loaded HZSM-5 Zeolites. *J. Energy Inst.* **2020**, *93*, 605–613. [CrossRef]
12. Tian, H.; Zhu, R.; Chen, L.; Wang, J.; Cheng, Y. Aromatic Hydrocarbons Rich Bio-Oil Production from Miscanthus Pyrolysis by Coupling Torrefaction and MoO3/ZSM-5 Dual Catalysis Process. *Ind. Crops Prod.* **2023**, *204*, 117314. [CrossRef]
13. Bridgwater, A.V. Review of Fast Pyrolysis of Biomass and Product Upgrading. *Biomass Bioenergy* **2012**, *38*, 68–94. [CrossRef]
14. Fernandez, E.; Amutio, M.; Artetxe, M.; Lopez, G.; Santamaria, L.; Lopez, J.E.; Olazar, M.; Saldarriaga, J.F. Exploring the Potential of Fast Pyrolysis of Invasive Biomass Species for the Production of Chemicals. *J. Anal. Appl. Pyrolysis* **2024**, *183*, 106817. [CrossRef]
15. Zong, P.; Jiang, Y.; Tian, Y.; Li, J.; Yuan, M.; Ji, Y.; Chen, M.; Li, D.; Qiao, Y. Pyrolysis Behavior and Product Distributions of Biomass Six Group Components: Starch, Cellulose, Hemicellulose, Lignin, Protein and Oil. *Energy Convers. Manag.* **2020**, *216*, 112777. [CrossRef]
16. Liu, S.; Zhao, W.; He, Z.; Yin, M.; Yao, J.; Yi, W. Effect of CO_2-Rich Atmosphere on Nitrogen Configuration of Char and Bio-Oil during Nitrogen-Rich Pyrolysis of Cellulose. *J. Energy Inst.* **2024**, *113*, 101501. [CrossRef]
17. Alcazar-Ruiz, A.; Dorado, F.; Sanchez-Silva, L. Influence of Temperature and Residence Time on Torrefaction Coupled to Fast Pyrolysis for Valorizing Agricultural Waste. *Energies* **2022**, *15*, 7914. [CrossRef]
18. Mo, F.; Ullah, H.; Zada, N.; Shahab, A. A Review on Catalytic Co-Pyrolysis of Biomass and Plastics Waste as a Thermochemical Conversion to Produce Valuable Products. *Energies* **2023**, *16*, 5403. [CrossRef]
19. Sabino, J.; Liborio, D.O.; Arias, S.; Gonzalez, J.F.; Barbosa, C.M.B.M.; Carvalho, F.R.; Frety, R.; Barros, I.C.L.; Pacheco, J.G.A. Hydrogen-Free Deoxygenation of Oleic Acid and Industrial Vegetable Oil Waste on CuNiAl Catalysts for Biofuel Production. *Energies* **2023**, *16*, 6131. [CrossRef]
20. Le, T.A.; Ly, H.V.; Kim, J.; Kim, S.-S.; Choi, J.H.; Woo, H.-C.; Othman, M.R. Hydrodeoxygenation of 2-Furyl Methyl Ketone as a Model Compound in Bio-Oil from Pyrolysis of Saccharina Japonica Alga in Fixed-Bed Reactor. *Chem. Eng. J.* **2014**, *250*, 157–163. [CrossRef]
21. Tan, H.; Rong, S.; Zhao, R.; Cui, H.; Zhang, N.-N.; Chen, Z.-N.; Li, Z.; Yi, W.; Zhang, F. Targeted Conversion of Model Phenolics in Pyrolysis Bio-Oils to Arenes via Hydrodeoxygenation over MoOx/BaO@SBA-15 Catalyst. *Chem. Eng. J.* **2022**, *438*, 135577. [CrossRef]
22. Wei, X.; Cao, Y.; Li, J. Synergistic Effect of Acid Sites and a Gallium-Based Modified Meso-/Microporous Catalyst for the Pyrolysis of Biomass. *Renew. Energy* **2022**, *191*, 580–590. [CrossRef]
23. Yeboah, I.; Li, Y.; Rajendran, K.; Rout, K.R.; Chen, D. Tandem Hydrodeoxygenation Catalyst System for Hydrocarbons Production from Simulated Bio-Oil: Effect of C–C Coupling Catalysts. *Ind. Eng. Chem. Res.* **2021**, *60*, 2136–2143. [CrossRef]
24. Martínez-Klimov, M.E.; Mäki-Arvela, P.; Vajglova, Z.; Alda-Onggar, M.; Angervo, I.; Kumar, N.; Eränen, K.; Peurla, M.; Calimli, M.H.; Muller, J.; et al. Hydrodeoxygenation of Isoeugenol over Carbon-Supported Pt and Pt–Re Catalysts for Production of Renewable Jet Fuel. *Energy Fuels* **2021**, *35*, 17755–17768. [CrossRef]
25. Oh, S.; Hwang, H.; Choi, H.S.; Choi, J.W. The Effects of Noble Metal Catalysts on the Bio-Oil Quality during the Hydrodeoxygenative Upgrading Process. *Fuel* **2015**, *153*, 535–543. [CrossRef]
26. Yao, G.; Wu, G.; Dai, W.; Guan, N.; Li, L. Hydrodeoxygenation of Lignin-Derived Phenolic Compounds over Bi-Functional Ru/H-Beta under Mild Conditions. *Fuel* **2015**, *150*, 175–183. [CrossRef]
27. Cheng, S.; Wei, L.; Julson, J.; Rabnawaz, M. Upgrading Pyrolysis Bio-Oil through Hydrodeoxygenation (HDO) Using Non-Sulfided Fe-Co/SiO2 Catalyst. *Energy Convers. Manag.* **2017**, *150*, 331–342. [CrossRef]
28. Saidi, M.; Safaripour, M. Aqueous Phase Hydrodeoxygenation of Anisole as a Pyrolysis Lignin-Derived Bio-Oil by Ether-Functionalized Ionic Polymer-Stabilized Ni-Mo Nanocatalyst. *Sustain. Energy Technol. Assess.* **2022**, *49*, 101770. [CrossRef]
29. Shi, W.; Gao, Y.; Song, S.; Zhao, Y. One-Pot Conversion of Bio-Oil to Diesel- and Jet-Fuel-Range Hydrocarbons in Supercritical Cyclohexane. *Ind. Eng. Chem. Res.* **2014**, *53*, 11557–11565. [CrossRef]
30. Koike, N.; Hosokai, S.; Takagaki, A.; Nishimura, S.; Kikuchi, R.; Ebitani, K.; Suzuki, Y.; Oyama, S.T. Upgrading of Pyrolysis Bio-Oil Using Nickel Phosphide Catalysts. *J. Catal.* **2016**, *333*, 115–126. [CrossRef]
31. Wang, Y.; He, T.; Liu, K.; Wu, J.; Fang, Y. From Biomass to Advanced Bio-Fuel by Catalytic Pyrolysis/Hydro-Processing: Hydrodeoxygenation of Bio-Oil Derived from Biomass Catalytic Pyrolysis. *Bioresour. Technol.* **2012**, *108*, 280–284. [CrossRef] [PubMed]
32. Yang, S.; Chen, G.; Guan, Q.; Xu, H.; Wang, Z.; Liu, B.; Yang, S.; Lei, T.; Zeng, X.; Lin, L. An Efficient Pd/Carbon-Silica-Alumina Catalyst for the Hydrodeoxygenation of Bio-Oil Model Compound Phenol. *Mol. Catal.* **2021**, *510*, 111681. [CrossRef]
33. Zhang, X.; Tang, W.; Zhang, Q.; Wang, T.; Ma, L. Hydrodeoxygenation of Lignin-Derived Phenoic Compounds to Hydrocarbon Fuel over Supported Ni-Based Catalysts. *Appl. Energy* **2018**, *227*, 73–79. [CrossRef]
34. Lin, X.; Kong, L.; Cai, H.; Zhang, Q.; Bi, D.; Yi, W. Effects of Alkali and Alkaline Earth Metals on the Co-Pyrolysis of Cellulose and High Density Polyethylene Using TGA and Py-GC/MS. *Fuel Process. Technol.* **2019**, *191*, 71–78. [CrossRef]

35. Wang, J.; Zhang, B.; Zhong, Z.; Ding, K.; Deng, A.; Min, M.; Chen, P.; Ruan, R. Catalytic Fast Co-Pyrolysis of Bamboo Residual and Waste Lubricating Oil over an Ex-Situ Dual Catalytic Beds of MgO and HZSM-5: Analytical PY-GC/MS Study. *Energy Convers. Manag.* **2017**, *139*, 222–231. [CrossRef]
36. Lin, X.; Zhang, Z.; Zhang, Z.; Sun, J.; Wang, Q.; Pittman, C.U. Catalytic Fast Pyrolysis of a Wood-Plastic Composite with Metal Oxides as Catalysts. *Waste Manag.* **2018**, *79*, 38–47. [CrossRef]
37. Long, J.; Shu, S.; Wu, Q.; Yuan, Z.; Wang, T.; Xu, Y.; Zhang, X.; Zhang, Q.; Ma, L. Selective Cyclohexanol Production from the Renewable Lignin Derived Phenolic Chemicals Catalyzed by Ni/MgO. *Energy Convers. Manag.* **2015**, *105*, 570–577. [CrossRef]
38. Rehman, M.U.; Wang, H.; Chawla, M.; Liu, W.; Lu, X.; Wang, S.; Xu, Y.; Wang, S.; Zhao, Y. Hydrodeoxygenation of Phenol to Cyclohexane over Bimetallic NiMo/CeO_2 Supported Catalysts: Tuning of Lewis Acid Sites by Mo Promotion. *Chem. Eng. J.* **2025**, *505*, 159407. [CrossRef]
39. Li, S.; Liu, B.; Truong, J.; Luo, Z.; Ford, P.C.; Abu-Omar, M.M. One-Pot Hydrodeoxygenation (HDO) of Lignin Monomers to C9 Hydrocarbons Co-Catalysed by Ru/C and Nb_2O_5. *Green Chem.* **2020**, *22*, 7406–7416. [CrossRef]
40. Leal, G.F.; Lima, S.; Graça, I.; Carrer, H.; Barrett, D.H.; Teixeira-Neto, E.; Curvelo, A.A.S.; Rodella, C.B.; Rinaldi, R. Design of Nickel Supported on Water-Tolerant Nb_2O_5 Catalysts for the Hydrotreating of Lignin Streams Obtained from Lignin-First Biorefining. *iScience* **2019**, *15*, 467–488. [CrossRef]
41. Gollakota, A.R.K.; Shu, C.-M.; Sarangi, P.K.; Shadangi, K.P.; Rakshit, S.; Kennedy, J.F.; Gupta, V.K.; Sharma, M. Catalytic Hydrodeoxygenation of Bio-Oil and Model Compounds-Choice of Catalysts, and Mechanisms. *Renew. Sustain. Energy Rev.* **2023**, *187*, 113700. [CrossRef]
42. Sui, H.; Shao, J.; Agblevor, F.A.; Zhang, Y.; Wang, X.; Yang, H.; Chen, H. Fractional Condensation and Aging of Pyrolysis Oil from Cotton Stalk. *Biomass Bioenergy* **2023**, *174*, 106837. [CrossRef]
43. Pereira, L.G.G.; Yuan, Q.; Heeres, H.J.; Lima, S.B.; Pires, C.A.M. Catalytic Hydrotreatment of Fast Pyrolysis Oils Using Ni-Cu/Al-MCM-41 Catalysts. *J. Anal. Appl. Pyrolysis* **2024**, *181*, 106593. [CrossRef]
44. Zhang, W.; Wang, Z.; Ge, T.; Yang, C.; Song, W.; Li, S.; Ma, R. Catalytic Pyrolysis of Corn Straw for Deoxygenation of Bio-Oil with Different Types of Catalysts. *Korean J. Chem. Eng.* **2022**, *39*, 1240–1247. [CrossRef]
45. Wang, Z.-C.; Duo, J.; Shan, Y.-Q.; Yin, L.-X.; Duan, P.-G. Hydro-Upgrading of Bio-Oils Derived from Pyrolysis of Biomass with Different H/Ceff Ratios in Tetralin over Pt/C and Ru/C. *Int. J. Hydrogen Energy* **2023**, *48*, 6916–6926. [CrossRef]
46. Wang, Q.; Wu, K.; Yu, Z. Ruthenium(III)-Catalyzed β-Alkylation of Secondary Alcohols with Primary Alcohols. *Organometallics* **2016**, *35*, 1251–1256. [CrossRef]
47. Illam, P.M.; Rit, A. Electronically Tuneable Orthometalated Ru^{II} –NHC Complexes as Efficient Catalysts for C–C and C–N Bond Formations via Borrowing Hydrogen Strategy. *Catal. Sci. Technol.* **2022**, *12*, 67–74. [CrossRef]
48. Gao, D.; Schweitzer, C.; Hwang, H.T.; Varma, A. Conversion of Guaiacol on Noble Metal Catalysts: Reaction Performance and Deactivation Studies. *Ind. Eng. Chem. Res.* **2014**, *53*, 18658–18667. [CrossRef]
49. Zheng, Y.; Wang, J.; Li, D.; Liu, C.; Lu, Y.; Lin, X.; Zheng, Z. Highly Efficient Catalytic Pyrolysis of Biomass Vapors Upgraded into Jet Fuel Range Hydrocarbon-Rich Bio-Oil over a Bimetallic Pt–Ni/γ-Al_2O_3 Catalyst. *Int. J. Hydrogen Energy* **2021**, *46*, 27922–27940. [CrossRef]
50. Shrotri, A.; Tanksale, A.; Beltramini, J.N.; Gurav, H.; Chilukuri, S.V. Conversion of Cellulose to Polyols over Promoted Nickel Catalysts. *Catal. Sci. Technol.* **2012**, *2*, 1852. [CrossRef]
51. Liang, G.; He, L.; Arai, M.; Zhao, F. The Pt-Enriched PtNi Alloy Surface and Its Excellent Catalytic Performance in Hydrolytic Hydrogenation of Cellulose. *ChemSusChem* **2014**, *7*, 1415–1421. [CrossRef] [PubMed]
52. Shi, F.; Wang, H.; Chen, Y.; Lu, Y.; Hou, D.; Liu, C.; Lu, Y.; Lin, X.; Yang, X.; Zheng, Z.; et al. Green Diesel-like Hydrocarbon Production by H2-Free Catalytic Deoxygenation of Oleic Acid via Ni/MgO-Al_2O_3 Catalysts: Effect of the Metal Loading Amount. *J. Environ. Chem. Eng.* **2023**, *11*, 110520. [CrossRef]
53. Amanollahi, H.; Moussavi, G.; Ostovar, S.; Giannakis, S. From Waste to Wealth: Using MgO Nanoparticles to Transform Ammonium into a Valuable Resource. *J. Water Process Eng.* **2023**, *56*, 104331. [CrossRef]
54. Xu, Y.; Liu, Z.; Liu, B.; Dong, B.; Pan, Y.; Li, Y.; Li, Y.; Guo, H.; Chai, Y.; Liu, C. Regulation of Surface Hydrophobicity and Metal Dispersion on Pt-Based Catalyst for the Boosted Hydrodeoxygenation of Guaiacol into Bio-Hydrocarbons. *Mol. Catal.* **2024**, *553*, 113761. [CrossRef]
55. Motin, A.M.; Haunold, T.; Bukhtiyarov, A.V.; Bera, A.; Rameshan, C.; Rupprechter, G. Surface Science Approach to Pt/Carbon Model Catalysts: XPS, STM and Microreactor Studies. *Appl. Surf. Sci.* **2018**, *440*, 680–687. [CrossRef]
56. Grosvenor, A.P.; Biesinger, M.C.; Smart, R.S.C.; McIntyre, N.S. New Interpretations of XPS Spectra of Nickel Metal and Oxides. *Surf. Sci.* **2006**, *600*, 1771–1779. [CrossRef]
57. Zhang, W.; Li, B. Electrochemical Properties and XPS Analysis of Ni-B/SiC Nanocomposite Coatings. *Int. J. Electrochem. Sci.* **2018**, *13*, 3516–3526. [CrossRef]
58. Li, H.; Ma, H.; Zhao, W.; Li, X.; Long, J. Upgrading Lignin Bio-Oil for Oxygen-Containing Fuel Production Using Ni/MgO: Effect of the Catalyst Calcination Temperature. *Appl. Energy* **2019**, *253*, 113613. [CrossRef]

59. Gholinejad, M.; Khosravi, F.; Sansano, J.M.; Vishnuraj, R.; Pullithadathil, B. Bimetallic AuNi Nanoparticles Supported on Mesoporous MgO as Catalyst for Sonogashira-Hagihara Cross-Coupling Reaction. *J. Organomet. Chem.* **2023**, *987–988*, 122636. [CrossRef]
60. Li, W.; Pan, C.; Zhang, Q.; Liu, Z.; Peng, J.; Chen, P.; Lou, H.; Zheng, X. Upgrading of Low-Boiling Fraction of Bio-Oil in Supercritical Methanol and Reaction Network. *Bioresour. Technol.* **2011**, *102*, 4884–4889. [CrossRef]
61. Recombinant Lactic Acid Bacterial Cell Useful for Producing 2,3-Butanediol, Comprises Gene Encoding Heterologous Polypeptide Having Butanediol Dehydrogenase Activity, Where the Bacterial Cell Is Free of Lactate Dehydrogenase Activity-All Databases. Available online: https://webofscience.clarivate.cn/wos/alldb/full-record/DIIDW:2010D87951 (accessed on 5 January 2024).
62. Nejadmoghadam, E.; Achour, A.; Öhrman, O.; Salam, M.A.; Creaser, D.; Olsson, L. Stabilization of Fresh and Aged Simulated Pyrolysis Oil through Mild Hydrotreatment Using Noble Metal Catalysts. *Energy Convers. Manag.* **2024**, *313*, 118570. [CrossRef]
63. Zheng, H.-Y.; Zhu, Y.-L.; Teng, B.-T.; Bai, Z.-Q.; Zhang, C.-H.; Xiang, H.-W.; Li, Y.-W. Towards Understanding the Reaction Pathway in Vapour Phase Hydrogenation of Furfural to 2-Methylfuran. *J. Mol. Catal. A Chem.* **2006**, *246*, 18–23. [CrossRef]
64. Merlo, A.B.; Vetere, V.; Ruggera, J.F.; Casella, M.L. Bimetallic PtSn Catalyst for the Selective Hydrogenation of Furfural to Furfuryl Alcohol in Liquid-Phase. *Catal. Commun.* **2009**, *10*, 1665–1669. [CrossRef]
65. Cheng, S.; Wei, L.; Julson, J.; Muthukumarappan, K.; Kharel, P.R.; Cao, Y.; Boakye, E.; Raynie, D.; Gu, Z. Hydrodeoxygenation Upgrading of Pine Sawdust Bio-Oil Using Zinc Metal with Zero Valency. *J. Taiwan Inst. Chem. Eng.* **2017**, *74*, 146–153. [CrossRef]
66. Cheng, S.; Wei, L.; Zhao, X.; Kadis, E.; Cao, Y.; Julson, J.; Gu, Z. Hydrodeoxygenation of Prairie Cordgrass Bio-Oil over Ni Based Activated Carbon Synergistic Catalysts Combined with Different Metals. *New Biotechnol.* **2016**, *33*, 440–448. [CrossRef]
67. Huang, Y.; Wei, L.; Zhao, X.; Julson, J.; Qiu, C.; Dharmarajan, S.; Kiratu, J.; Raynie, D.; Dubey, A.; Qiao, Q. Biofuel Production Using Pd/Zn Synergistically Catalyzed Hydrodeoxygenation Applied at Bio Oil Extracted in Biomass Pyrolysis Process: Hydrodeoxygenation for Green Fuel. *Int. J. Energy Res.* **2016**, *40*, 1724–1730. [CrossRef]
68. Joshi, R.M.; Pegg, M.J. Flow Properties of Biodiesel Fuel Blends at Low Temperatures. *Fuel* **2007**, *86*, 143–151. [CrossRef]
69. Patel, M.; Kumar, A. Production of Renewable Diesel through the Hydroprocessing of Lignocellulosic Biomass-Derived Bio-Oil: A Review. *Renew. Sustain. Energy Rev.* **2016**, *58*, 1293–1307. [CrossRef]
70. Shi, J.; Luo, Z.; Sun, H.; Qian, Q.; Wei, Q.; Li, L. Enhancing Corn Stover to Bio-Jet Fuel Process: Valorizing Lignin-Enriched Residue for Energy, Economic, and Environmental Benefits. *Biomass Bioenergy* **2024**, *188*, 107338. [CrossRef]